SOURCE ROCK OVERPRESSURE PREDICTION AND ITS RELATION TO KEROGEN MATURITY

A Thesis

by

CHRISTOPHER AUSTIN VILLARREAL

Submitted to the Office of Graduate and Professional Studies of
Texas A&M University
in partial fulfillment of the requirements for the degree of

MASTER OF SCIENCE

Chair of Committee,	Ibrahim Yucel Akkutlu
Committee Members,	Ruud Weijermars
	John Pantano
Head of Department,	A. Daniel Hill

August 2016

Major Subject: Petroleum Engineering

Copyright 2016 Christopher Villarreal

ABSTRACT

Accurate formation pressure estimation is important to drilling and production operations and necessary for reservoir engineering calculations. Methods developed to estimate formation pressure from well logs are reliable for conventional reservoirs but do not translate well to unconventionals. Due to a limited hydraulic connectivity between the organic matter (kerogen) pore network and the inorganic matrix pore network holding the stored hydrocarbons, current methods may not accurately estimate the magnitude of overpressure in source rocks and unconventional targets in mature basins.

In this work, a pressure estimation method is developed mainly using data from porosity logs. The proposed method is applied to areas in the Delaware Basin to demonstrate the presence of overpressure in the Bone Spring Sands and Wolfcamp formation. Validation pressure measurements based on DST, flowback, and managed pressure drilling data through multiple horizons indicate the weak transport coupling of the 3rd Bone Spring Sands and Wolfcamp horizons while also demonstrating a reliable method to estimate formation pressures using sonic well logs. The estimated overpressures in the Delaware Basin demonstrate a strong correlation with previously measured kerogen maturity and indicate that hydrocarbon generation is the significant source of the recognized present day overpressure.

ACKNOWLEDGEMENTS

I wish to express my greatest thanks to Joseph Foran and the outstanding team he assembled at Matador Resources. The opportunity to work in a group as driven and committed to excellence as Matador has been the opportunity of a lifetime. Herman Collette's guidance was instrumental in this project's idea development and completion. I would also like to thank Dr. Akkutlu for his significant support and mentorship over the course of the study. His willingness to question general conventions and consider methods that go against "the way things have always been done" were critical to this project's execution.

Thank you to the State of Texas and the VA for allowing me to study petroleum engineering with the Hazelwood Act and the GI Bill. Finally, thank you to the officers and non-commissioned officers whose life lessons in grit and resiliency were instrumental in the completion of this project. COL Getchell, COL Dooghan, LTC Phillips, 1SG Murillo, SFC Clanin, and SFC Delgado were all profound factors in helping me learn what it takes to accomplish the missions that initially seem impossible.

NOMENCLATURE

CALD_A2D	=	Caliper log [in]
D	=	Depth [ft]
$D_{maximum}$	=	Maximum depth [ft]
DST	=	Drill stem test [-]
DT_A2D	=	Compressional sonic transit time [μs/ft]
EC:	=	Environmentally corrected log [-]
EC:GR	=	Environmentally corrected gamma ray log [gamma ray API units, GAPI]
EC:PE	=	Environmentally corrected photoelectric log [Barnes/electron]
EC:NPHI	=	Environmentally corrected neutron porosity curve [decimal]
EC:RHOB	=	Environmentally corrected bulk density log [g/cm^3]
g	=	Acceleration due to gravity [ft/sec^2]
Gen:HydStat	=	User generated hydrostatic pressure [psi]
Gen:HydStatGrad	=	User generated hydrostatic gradient [psi/ft]
Gen:NCT	=	User generated normal compaction trend in shale [μs/ft]
Gen:NCT_Sand	=	User generated normal compaction trend in sand [μs/ft]
Gen:OB_Gradient	=	User generated overburden gradient [psi/ft]
Gen:Overburden	=	User generated overburden pressure [psi]
Gen:PorePressure	=	User generated pore pressure from shale normal compaction trend [psi]

Gen:PorePressure_Sand	=	User generated pore pressure from sand normal compaction trend [psi]
LOM	=	Level of maturity [-]
MPD	=	Managed pressure drilling [-]
NCT	=	Normal compaction trend [μs/ft]
OB	=	Overburden pressure [lbf/in^2, psi]
P	=	Pressure [psi]
P_{atm}	=	Atmospheric pressure [psi]
P_{csg}	=	Casing pressure [psi]
P_{Hydro}	=	Hydrostatic pressure [psi]
P_i	=	Initial reservoir pressure [psi]
P_{Norm}	=	Normal pore pressure [psi]
P_{wf}	=	Bottom hole flowing pressure [psi]
R	=	Observed resistivity [ohm-m]
$R_{baseline}$	=	Baseline resistivity [ohm-m]
Ro	=	Vitrinite reflectance [%]
$Temp_{AreaAvg}$	=	Area's average temperature [°F]
$Temp_{max}$	=	Maximum temperature [°F]
TOC	=	Total organic carbon [wt%]
TOC:DTovl	=	The scaled sonic input curve for Passey's ΔLogR method [μs/ft]
TOC:LogRT	=	The scaled resistivity input curve for Passey's ΔLogR method [-]
TOC:NPHIovl	=	The scaled neutron porosity input curve for Passey's

		ΔLogR method [decimal]
TOC:RHOBovl	=	The scaled bulk density input curve for Passey's ΔLogR method [gm/cm^3]
TOC:TOC	=	The average of the sonic, density, and neutron ΔLogR overlays [wt%]
TOC:TOC_DLRD	=	The calculated TOC from the density-ΔLogR overlay [wt%]
TOC:TOC_DLRN	=	The calculated TOC from the neutron-ΔLogR overlay [wt%]
TOC:TOC_DLRS	=	The calculated TOC from the sonic-ΔLogR overlay [wt%]
TopDepth	=	Depth of the top of the bulk density curve [ft]
TVD	=	Total vertical depth [ft]
W_{mud}	=	Mud weight [lbf/gal]

Greek Letters:

$\Delta logR_{Den}$	=	Passey's delta log R based on the bulk density and resistivity curves [-]
$\Delta logR_{Neu}$	=	Passey's delta log R based on the neutron and resistivity curves [-]
$\Delta logR_{Sonic}$	=	Passey's delta log R based on the sonic and resistivity curves [-]
ΔP	=	Overpressure [psi]
$\Delta P_{friction}$	=	Frictional pressure loss [psi]
$\Delta T_{baseline}$	=	Baseline compressional sonic travel time [μs/ft]
ΔT_{norm}	=	Normal compressional sonic travel time [μs/ft]
ΔT_{ob}	=	Observed compressional sonic travel time [μs/ft]

ρ_{app}	=	Apparent density [g/cm^3]
ρ_b	=	Bulk density [g/cm^3]
$\rho_{baseline}$	=	Baseline bulk density [g/cm^3]
ρ_f	=	Fluid density [g/cm^3]
ρ_m	=	Matrix density [g/cm^3]
ρ_w	=	Density of water [lbf/ft^3]
σ	=	Matrix stress [psi]
φ	=	Porosity [decimal]
ϕN	=	Observed neutron porosity [decimal]
$\phi N_{baseline}$	=	Baseline neutron porosity [decimal]
∇P_{water}	=	Water pressure gradient [psi/ft]

TABLE OF CONTENTS

Page

LIST OF FIGURES

Page

LIST OF TABLES

Page

1. INTRODUCTION

Petroleum exploration and production companies constantly seek new methods to drill better performing wells, in less time and for less money. These companies achieve this objective by relying on expert knowledge and leveraging technology. But, the necessary knowledge can be overwhelming during operations in new formations and in new regions. Understanding pressures ultimately plays an important role in achieving production goals. Formation pressures are a key piece in models used to build strategic basin development plans. The magnitude, location, and causes of formation overpressure all factor into effective basin models. Companies seek to understand formation pressures and pressure trends in order to optimize casing design, select appropriate mud weights during drilling, and help guide exploration decisions. This thesis aims to expand on established methods for estimating formation pressures using well logs, develop an effective method to identify and estimate overpressure formations within a basin, and determine the probable cause of the recognized overpressure.

Understanding the pressure distribution in the basin is critical to an exploration and production (E&P) company for a multitude of reasons. The overriding economic factor is that this knowledge allows the operator to optimize a drilling plan, specifically the number of intermediate casing strings required for the well. Next, knowing formation pressures will also enable drillers to better gauge required mud weights. Overestimating the formation pressure could lead to an unnecessarily heavy mud being used, which risks formation fracturing and lost circulation while drilling. Underestimating the formation pressure and using a lighter mud weight could lead to fluid influx and well control issues.

Additionally, the pressure and porosity measurements are closely tied. If the overpressure is a result of the kerogen maturation process, then the degree of overpressure can be related to maturity. Total Organic Carbon (TOC), maturity and lithology can be combined to separate out organic porosity from the total porosity.

Economically, pressures can play a much greater role outside the drilling and production realms if they are utilized for reserves calculations and lease acquisitions. Mapped areas of overpressure can reveal locations to target for future acreage acquisitions and possibly highlight bargain acreage positions that may contain overpressured formations but are away from the current high cost lease areas. However, while pressure plays an important factor in the success probability of a well, it is certainly not the only factor. As engineers and geologists resolve the additional factors impacting a well's estimated ultimate recovery (EUR) in specific areas of a basin, they will be able to utilize pressure maps to help tune their models to predict EUR and classify reserves. Therefore, the ability to accurately estimate pressures can play a direct role in a company being able to acquire better acreage and book more reserves which will increase the company's value.

1.1 Formation Pressure

In the context of this study and petroleum engineering as a whole, overpressure is when the pore pressure within a given formation exceeds the hydrostatic pressure. For basic estimates, industry generally assumes a normal hydrostatic pressure gradient of approximately 0.465 psi/ft, which corresponds to a brine density of 8.95 lbm/gal. For reference, freshwater has a density of 8.33 lbm/gal, which translates to a 0.433 psi/ft pressure gradient.

In normally pressured basins, the porosity usually decreases with depth because of the increasing overburden stress, which compresses the formation and reduces the pore volume. Hence, the overburden stress tends to compact the rock and squeeze out any fluids present in the pores.

Based off of the work of Terzaghi and Peck (Terzaghi et al., 1996), Hottmann and Johnson (1965) developed an effective illustration to model the pressure process. They show a cup holding water with submerged springs covered by a flat metal plate with an outer diameter equal to the cup's inner diameter. A constant external load, P_{OB}, is applied to the top of the plate. This load is analogous to the overburden pressure. Whereas the springs are an analog for the matrix. If no fluid is allowed to escape, as shown in cup A in **Figure 1.1**, then the system is overpressured and the fluid takes on a greater portion of the total force opposing load P_{OB}. Cup B is analogous to a formation undergoing compaction and the fluid is escaping from the pore as the overburden pressure is applied. The springs are taking on a greater portion of the overburden pressure as water leaves the cup. If fluid is allowed to escape until the pressures exerted by the springs and fluid reach equilibrium with the applied overburden pressure, then the system is said to be in compaction equilibrium and normally pressured.

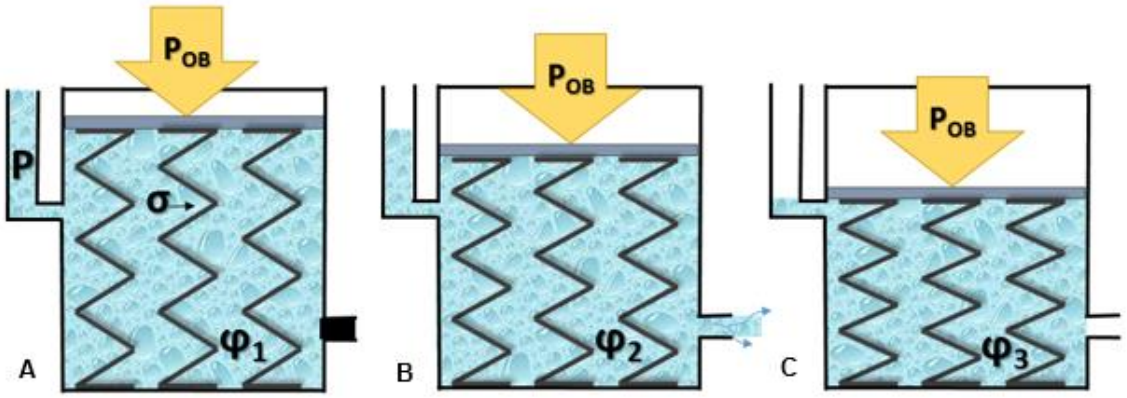

Figure 1.1. Pore pressure illustration adapted from Hottmann and Johnson (1965) and Terzaghi et al. (1996)

Hence, it can be seen that:

$$P_{OB} = \sigma + p \tag{1.1}$$

Meaning that overburden pressure, P_{OB}, equals the stress (σ) the matrix is experiencing plus the pressure (p) exerted by the fluids residing in the matrix pores.

In formations open to atmospheric conditions, the pore pressure is equal to the hydrostatic pressure at a particular depth and is a function of the weight of the fluid column. This is the case for normally pressured formations. If the formation pore pressure is greater than the hydrostatic pressure, the formation is said to be overpressured. For a normally pressured water bearing formation, the pore pressure can be calculated as a function of the density of water (ρ_w), gravitational acceleration (g), and vertical depth (D).

The hydrostatic pressure (P_{Hydro}) is calculated as:

$$P_{Hydro} = \rho_w \times g \times D \tag{1.2}$$

The example in **Figure 1.1** highlights the role overburden pressure plays in the pore pressure magnitude. The overburden pressure is the pressure that results from the cumulative weight of the rock matrix and the fluid overlaying the formation at the measured depth. In the most general case, the total magnitude of the overburden pressure (P_{OB}) at a particular depth can be calculated with the following equation:

$$P_{OB} = \rho_b \times g \times D \tag{1.3}$$

Where ρ_b represents the bulk density of the water saturated rock. Classically, bulk density is calculated as the porosity-weighted average of the pore fluid and solid matrix density values:

$$\rho_b = \varphi\rho_f + (1 - \varphi)\rho_m \tag{1.4}$$

Where φ represents porosity, ρ_f is fluid density, and ρ_m is matrix density.

1.2 Formation Pressures Measurements

Given the knowledge of how the pressures in the rock interact and how they are calculated, it is important to develop an understanding of how formation pressures are measured in the field.

1.2.1 Drill Stem Test

A drill stem test (DST) is a conventional way to measure formation pressure. DST equipment is typically set up as part of the bottom hole assembly on the drill stem or tubing and run into the well bore. Two packers on the testing instrument isolate the region of the formation under investigation. Prior to starting the test, the well is flowed. A gauge in the instrument in the bottom hole assembly measures the pressure while the tool is in operation. After the packers are set, the tool is opened and the gauge measures the flowing pressure. The tool is then shut and the gauge measures the pressure buildup as the formation begins to flow into the isolated wellbore region. This period is known as the initial shut in period. Shut in times are typically up to two hours for open hole, high permeability formations and can last over 5 days for tight formations in a perforated cased hole. Horner plots are typically used to interpret DST results by extrapolating the shut in period's recorded pressure trend out to an infinitely long shut in time in order to determine the initial reservoir pressure.

DST data is widely available from scout cards through various databases. Though, the accuracy of these measurements may be uncertain and there is generally not enough data for direct interpretations using the Horner plot. Additionally, in very low permeability formations, if the tool is not left in place long enough during the shut in period, the formation pressure trend will not be established enough to project static formation pressure. In these circumstances, the shut in pressure may be less than the actual reservoir pressure.

1.2.2 Wireline Pressure Measurements

Various wireline tools have been developed to estimate formation pressures at multiple depths along the wellbore. Schlumberger makes two of the most well-known varieties, the Repeat Formation Test and the PressureXpress (abbreviated by Schlumberger as XPT). These tools measure the sand face pressure by pressing a packer up against the borehole wall to isolate a probe against the formation. The tool operator then controls the volume and rate at which to pull from the formation. In very low permeability formations, small volumes in the range of 1.0 cm^3 can be used to enable more timely measurements.

One of the distinct advantages of wireline tools is that they allow for multiple measurements within a generally short duration of testing time. Additionally, specific depths, generally down to the half foot, can be located and tested. But, the downside is that formation heterogeneity and borehole conditions can greatly impact the success rate of the tool. A rugged hole, fractures on the borehole wall, or debris on the face of the packer can inhibit the packer from achieving the seal necessary for a valid pressure measurement. In addition, given that the testing probe is less than an inch in diameter, the tools are susceptible to measuring pressures on formation heterogeneities that are sub-resolution of most logging equipment. As with many tools in the oil field, the performance is in large part dependent on the tool operator's skill level. Leaving the tool in place too long can lead to it becoming stuck to the formation wall. Pulling away from the wall too early leads to pressure underestimation. Thus, the operator is in a constant balancing act between the necessity for reliable measurements and the financial risk associated with a stuck tool.

1.2.3 Managed Pressure Drilling

Managed pressure drilling (MPD) is a method of drilling commonly utilized in areas where a narrow window exists between the formation fracture gradient and the pore pressure gradient. During MPD, the drillers flow the mud returns through the choke, rather than the flowline. Drillers control formation inflow in the well with the mud weight and by maintaining casing pressure at the surface with the chokes. When the mud is circulating during drilling operations, the bottom hole pressure can be estimated as the hydrostatic weight of the mud column plus the equivalent circulating density (ECD). ECD accounts for the increased bottom hole pressure created by the annular fluid friction of the circulating mud in addition to the pressure from the mud's static fluid density. Thus, the bottom of the well experiences a higher mud weight when the pumps are circulating than when the pumps are switched off, such as during a drill pipe connection. When drilling in narrow windows between pore pressure gradients and fracture gradients, maintaining the bottom hole pressure via the chokes on the surface during drill pipe connections allows for drillers to compensate for the loss of ECD much more efficiently than adjusting the mud weight. During MPD, an increase in casing pressure during connections indicates that the well is flowing. So, the casing pressure during connections while drilling a horizontal lateral can be used as an indication of reservoir pressure if the casing is set in a hydraulically coupled formation.

Figure 1.2 illustrates the operation of MPD. Case A is an example of a normal blowout preventer (BOP) on the surface during normal drilling operations. The mud is circulating up the annulus, through the BOP and to the flowline where it will return into

the mud circulating system. The rotating head isolates the mud column and holds back pressure on annulus. During connections, the static weight of the mud column is enough to hold back flow from the formation. In Case B, the well is being drilled with MPD. At the instant pictured, the driller is making a connection so the mud is not circulating. Gas is flowing from the formation to the surface. The rotating head is isolating the annulus from the surface and the orbit valve is closed. The choke valve is opened so that the mud and gas flow to the casing pressure gauge, the chokes, and then the gas buster. The gas buster then sends the gas to be flared and returns the mud to the mud circulation system. The gas applying pressure on the chokes is applying equal pressure to the mud column behind it. This pressure is transmitted to the formation at the bottom of the hole. Once the pressure applied at the chokes is enough to cause the bottom hole pressure to equal the formation pore pressure, the flow from the formation ceases.

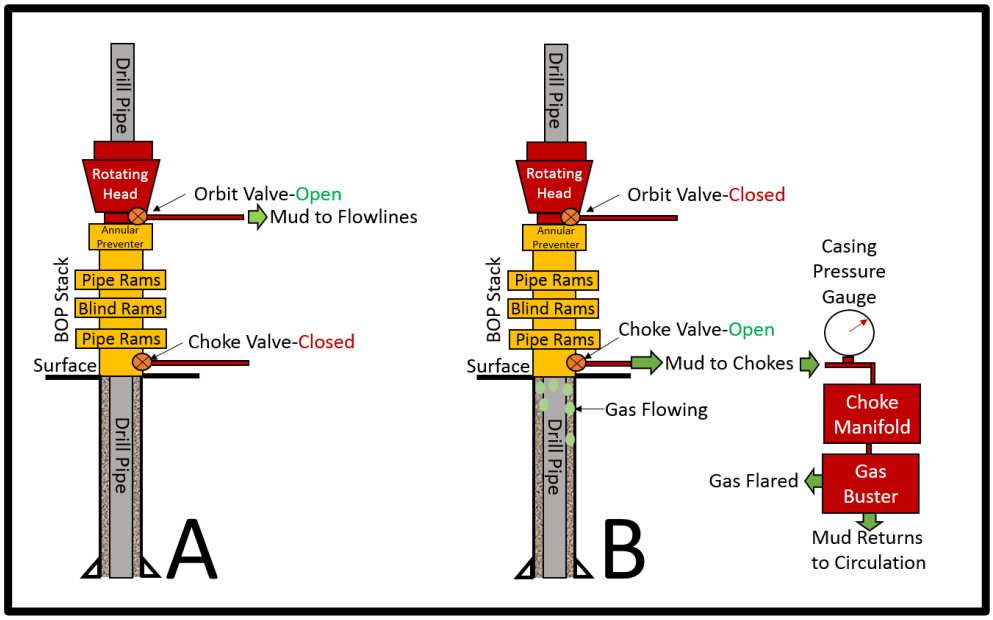

Figure 1.2. Managed pressure drilling operations

Figure 1.3 illustrates the MPD principles. At a depth corresponding to the end of the black arrow, the driller must decide on an appropriate mud weight moving forward. Mud B is heavier than Mud A. As shown by the green dot, Mud B would prevent the well from flowing during connections when the mud column is static, but it could fracture the formation while the mud is circulating during drilling due to the increased pressure from the ECD. Mud A would not fracture the formation while the mud is circulating, but formation fluid would flow into the wellbore during drill pipe connections when the mud is static in the wellbore. The differential between the hydrostatic pressure of Mud A and the pore pressure is nearly equivalent to the casing pressure at the surface during connections. Formation pressure can be calculated with the equation:

$$P_{wf} = P_{atm} + P_{csg} + 0.052 * TVD * W_{mud} \tag{1.5}$$

where P_{wf} is the bottom hole flowing pressure and estimated to be the initial reservoir pressure in psi, P_{atm} is atmospheric pressure and assumed to be 14.7 psi, P_{csg} is casing pressure in psi during connections, TVD is true vertical depth in feet, and W_{mud} is the drilling mud weight in lbm/gal.

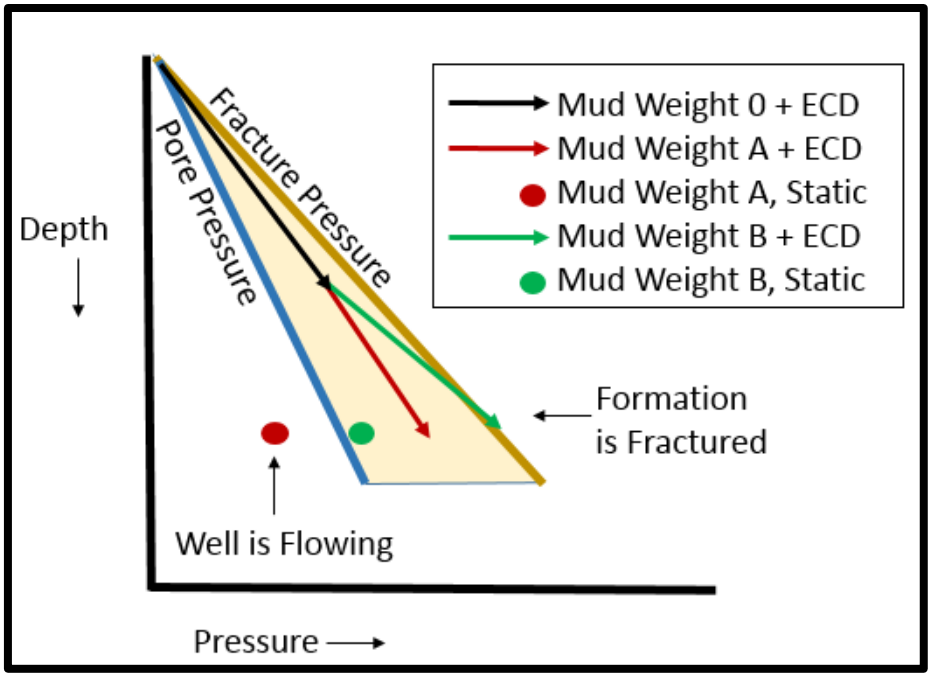

Figure 1.3. Simplified drilling pressure window with MPD illustrated

The original mud weight is illustrated as the black line as mud weight 0. At a certain depth, the drillers must decide whether to increase the mud weight. If mud weight B is used, the formation will fracture but the well will not flow when the borehole fluid is static while connecting drill pipe. If mud weight A is used, the formation will not fracture but the well will flow during connections. The flow can be held back at the chokes on surface and the formation pressure can be measured by the surface casing pressure.

1.2.4 Flowback Data

Jones et al. (2014) showed that hourly flowback data following the hydraulic fracturing (or frac) of a horizontal well could be used to estimate formation pressure. The underlying premise is that following completion, the well is still charged with pressure from the frac job. When flowback begins, the well flows predominately with the water that was injected during the frac job. During the early stages of flow back no hydrocarbons are flowing because the formation is seeking to expel the water that was forced into the fractures during the completion operation. Oil and gas do not begin to flow into the wellbore until the bottom hole pressure drops below the initial reservoir pressure. The

measured casing pressure at the surface starts out high and begins to level out as the induced pressure from the frac is bled off and the pressure in the lateral begins to reach reservoir pressure. At this point, the first traces of hydrocarbons begin to appear at the surface. The casing pressure will generally tend to decrease following the appearance of hydrocarbons at the surface as the fluid column in the well transitions to multiphase flow. At the appearance of the first hydrocarbons to the surface, the initial reservoir pressure can be estimated with the equation:

$$P_{wf} = P_{atm} + P_{csg} + \nabla P_{water} TVD + \Delta P_{friction} \tag{1.6}$$

where P_{wf} is bottom hole flowing pressure and assumed to be near the initial reservoir pressure in psi, P_{atm} is atmospheric pressure and assumed to be 14.7 psi, P_{csg} is casing pressure in psi, and ∇P_{water} is the pressure gradient of water in psi/ft. Based on salinity tests during flowback, 0.446 psi/ft is used for the study. TVD is true vertical depth in feet. $\Delta P_{friction}$ is the pressure loss due to friction on the production casing.

Some accuracy is lost in this calculation because the pressure is calculated based on a single phase vertical column of water. Because the pressure is taken at the first hydrocarbon appearance at the surface, the amount of hydrocarbon mixed with the water is assumed to be minimal and its effects are reduced. Accounting for the increased friction resulting from the wellbore's deviations from a perfectly straight and vertical hole would result in a higher bottom hole pressure but the effects are generally small enough that this calculation is outside the scope of this project.

1.3 Causes of Formation Overpressure

Overpressure is usually the result of one or a combination of three mechanisms. First, overpressure can result from a reduction in pore volume with an increased compressive stress caused by undercompaction or tectonics. Second, it may be caused by an increase in the pore fluid volume as a result of temperature increase, clay diagenesis, or hydrocarbon generation. Third, buoyant fluid movement through the formation may contribute to overpressure (Osborne and Swarbrick, 1997).

1.3.1 Pore Volume Change due to Compressional Stress

Undercompaction, also known as compaction disequilibrium, may refer to a situation where sedimentation occurs so rapidly that fluids within the pores do not have time to escape. As the sedimentation progresses, the overburden pressure continues to increase, which should correspond to a decrease in pore size. But, if the fluid did not have ample time to escape, the fluid carries some of the overburden stress rather than the matrix. For undercompaction to cause overpressure, a rapid burial rate must occur over top of low permeability sediments. This situation may also occur when overburden increases over time and compresses the pore volume by distorting the matrix material.

The required stratigraphy to maintain overpressure due to undercompaction can work to decrease the probability that it is the principle contributor to overpressured systems in some basins. Relevant to this project, Lee and Williams (2000) studied the plausibility of overpressure from undercompaction in the Delaware Basin. Overpressure in the Delaware Basin exists in sediments within areas up to 250 million years old. Through simulation, the authors determined that the seal capacity of the formation layers

above an overpressured layer would need to be exceptionally high in order to maintain the abnormal pressure for the time scope of concern in the Delaware Basin. The seals would be expected to be made of a low permeability shale or a sand sequence with dramatic calcite cementation. An overlying salt layer might hold the required pressure, but such layers are not seen in the basin immediately above identified overpressured areas.

Lee and Williams (2000) modeled the pressures in the Delaware Basin multiple ways. Assuming only 2-D flow, they found that a top pressure seal must have a continuous permeability of 10^{-11} darcy to maintain the overpressure for 250 million years. Most of the shales thus far studied have a permeability ranging between 10^{-4} to 10^{-8} darcy. Furthermore, the study found that even if only one-dimensional upward flow were possible, a 600 meter (1,968 ft.) thick, 10^{-9} darcy shale would only be able to maintain overpressure for about 200 million years. Because the basin is a 3-D system, the seal must also be able to trap pressure above, laterally and below the formation, without any vertical fractures. There is sufficient physical evidence of such fracture systems within the basin to indicate that this type of seal is not generally common in the areas of concern.

Lou et al. (1994) examined the sedimentation rates of the formations in the Delaware basin in the War-Wink field, as shown in **Figure 1.4**. Comparing the sedimentation rates to the measured overpressure from DSTs in **Figure 1.5**, a moderate correlation is seen in the overpressured formations and the elevated sedimentation rates of the overlaying formations. Specifically, according to Lou et al.'s pressure data, the Wolfcamp shows some of the greatest degrees of overpressure while also having the present day 763m

(2,503ft) thick Bone Spring formation over top of it, which had a generally rapid sedimentation rate of 207.8 meters/million years (or 682 ft/million years).

Table 1. Initial Sedimentation Rates, War-Wink Field*

Strata	Thickness (m) Present	Thickness (m) Initial	Duration (m.y.)	Initial Sedimentation Rate (m/m.y.)
Cenozoic	120	140.0	140	1.0
Jurassic	Absent	0 (?)	60	0.0
Triassic	180	190.5	50	3.8
Ochoa	1082	1225.1	5	245.0
Delaware Mt.	1057	1286.1	15	85.7
Bone Spring	763	1038.9	5	207.8
Wolfcampian	867	1354.9	15	90.3
Pennsylvanian	375	683.6	40	17.1
Barnett	155	212.9	10	21.3
Mississippian	290	437.1	15	29.1
Unconformity	0	-10.0 (?)	10	-1.0
Woodford	225	382.9	30	12.8
Unconformity	0	-10.0 (?)	10	-1.0
Silurian	138	193.0	15	12.9
Montoya	145	195.6	30	6.5
Simpson	420	655.0	30	21.8
Ellenburger	400	557.5	15	37.2

*Data are from burial history modeling results (Luo et al., 1993).

Figure 1.4. Delaware Basin sedimentation rate comparison, from Lou et al. (1994)

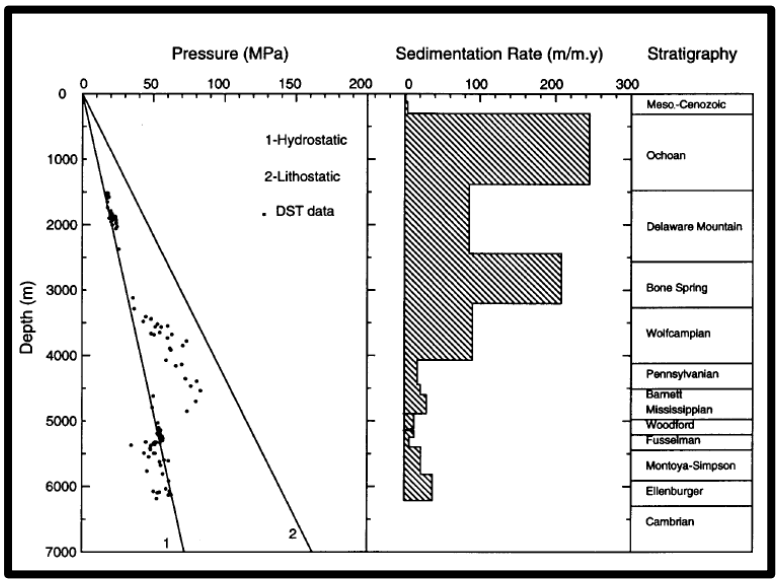

Figures 1.5. Delaware Basin sedimentation rate and overpressure comparison, from Lou et al. (1994)

The quantitative pressure data in Lou et al.'s study is used only to highlight the general overpressure trends. As discussed by Swarbrick (1995) and Cox (1995), Lou et al.'s reliance on the DST's initial and final hydrostatic pressures is not the optimal method for reliable inferences into reservoir pressure. A general trend in formation overpressures can be inferred from the hydrostatic pressure since mud weights are used as a means to offset this formation pressure. However, observed mud weights are often higher than necessary and thus trying to calculate the reservoir pressure from hydrostatic pressure will result in too high of a value. Lou and Baker (1995) contest that they applied corrections to the hydrostatic pressure, but without an exact methodology, their pressure measurements can be used only qualitatively.

Tectonic activity has a somewhat similar effect on pore fluid pressure as undercompaction. Overpressure as a result of tectonics can occur when movements along a fault compress the formation and increase the stress on the pores. This increased stress has the same effect as the vertical overburden stress. Though, often the increased stress may be accompanied with a new fracture network to help transport the pore fluid to a lower pressure zone. Understandably, overpressured systems from tectonic activity is most common in basins near major faults and tectonic boundaries.

1.3.2 Pore Fluid Volume Change

1.3.2.A Hydrocarbon Generation

Hydrocarbon generation can become a source of overpressure when dealing with source rocks. These rocks are rich in organic matter known as kerogen. Kerogen material is the driver of the hydrocarbon generation process. Pressure, temperature and time all

combine to advance kerogen maturity and the subsequent hydrocarbon generation. When kerogen matures, it generates hydrocarbon fluids. The fluid pressure increases during generation and leads to the expulsion of hydrocarbons from their initial positions. The mechanism of hydrocarbon generation from kerogen is controlled at the molecular level. Larger hydrocarbon molecules within the kerogen break into oil and gas. The kerogen becomes denser as the hydrogen atoms in its structure are utilized in the hydrocarbon generation process (Ward, 2010). The maturity progression can be seen on Van Krevelen's diagram in **Figure 1.6** with a decreasing H:C ratio as the kerogen matures. This ratio is a function of the molecular makeup of the expelled hydrocarbons. For example, alkanes all have a formula of C_nH_{2n+2}. So, each new hydrocarbon alkane molecule is taking away more hydrogen than carbon.

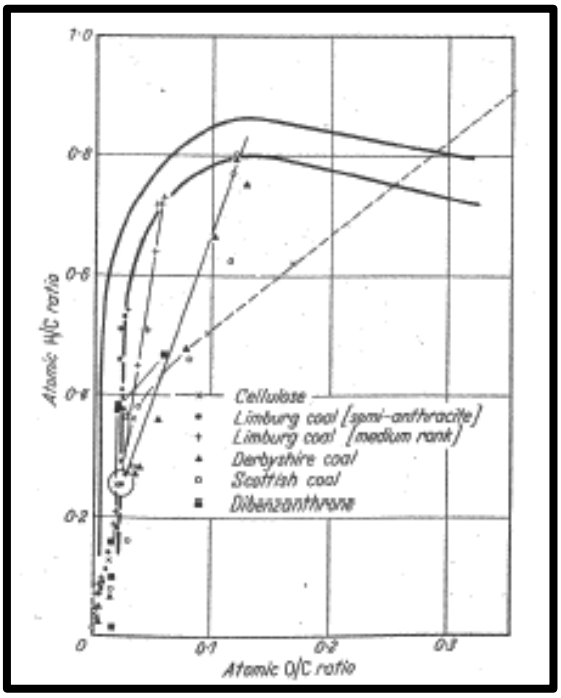

Figure 1.6. Van Krevelen's original diagram taken from Van Krevelen (1950)

Kerogen's maturity level can be estimated from its vitrinite reflectance in oil, Ro (not to be confused with Ra, the reflectance in air, which was common in the USSR). The Ro value represents the percentage of photons returning back to a measurement instrument after light is shined on a kerogen sample. Vitrinite reflectance generally falls on a scale of 0.2 to 3.0. Kerogen's decomposition products begin to be expelled immediately but the kerogen is not said to be in the peak oil window until Ro=0.8 and this window runs through Ro=1.2 (Vassoyevich et al. 1970). These Ro values are not concrete by any means. The scope of the Ro windows for oil and gas production is situationally dependent and there is valid reasoning for oil generation outside of this window and gas is generated through the entirety of kerogen decomposition. Though, this peak oil window is generally accepted as a rough left and right limit. The relative rate of gas expulsion is dependent on the original H:C ratio of the kerogen. Gas expulsion continues as the H:C ratio decreases with the polymerization within the kerogen beyond the oil window. As kerogen matures toward a graphite-type phase, the expelled gas increasingly shifts from a wet to dry gas. The kerogen develops pores as it expels the generated hydrocarbons. These pores eventually make up the organic porosity. Depending on how well they are interconnected, the organic pores can create an organic pore network. This network is largely separate from the conventional matrix porosity. However, this secondary organic network may combine with the conventional inorganic matrix pore network and fractures to contribute to the total porosity of the source rock formation.

The oil and gas leaving the kerogen have a much lower density than the kerogen itself. The greater volume occupied by the oil and gas will increase the pressure in the pores. If

the rock has adequate permeability, the increased pressure will cause the fluids to migrate out of the oil wet organic pores and into larger and more connected inorganic water wet matrix pores. This elevates the pressure within the inorganic matrix pores. If the formation is a sufficient capillary system, the generated hydrocarbons should then continue normal fluid migration. But, if the permeability is low enough that capillary effects are negligible then the increased internal pressure within the pore will press out on the walls and creates a pore volume that is above what would be expected at its given depth. In low permeability shales, the generated hydrocarbon fluids may not be able to escape and the pressure continues to build in the pore as the kerogen matures and expels more fluids. This can create an ultra-high pressure system within the kerogen rich shale. Traditional porosity measuring logging tools such as neutron porosity, bulk density, and sonic respond to this pore expansion caused by pressure and can thus be used as a tool to detect the occurrences of overpressure caused by kerogen maturation.

1.3.2.B Aqua-thermal Expansion

Aqua-thermal expansion refers to fluid expansion due to heating. If fluid is in a sealed container of constant volume, its pressure in the container will increase as the fluid is heated. Similar to under compaction, a nearly impermeable seal is needed to maintain the overpressure generated by greater fluid volumes due to aqua-thermal expansion. Lou and Vasseur (1992) conducted an exhaustive study in which they reduced the permeability of the sealing formation to 3×10^{-12} mD, adjusted their temperature gradient from 50°F/3,280ft to 122°F/3,280ft, and adjusted burial rates from 164 to 3,280 ft/million years. Through each trial, it was shown that aqua-thermal expansion contributed negligibly to

the overall generated overpressure. Additionally, Osborne and Swarbrick (1997) point out that overpressuring generally occurs gradually through a transition zone. But, a steady transition gradient implies permeability, which is incompatible with the requirements for aqua-thermal induced overpressure. So, while aqua-thermal expansion may play a role in overpressured systems, it is generally not the primary actor.

1.3.2.C Clay Diagenesis

Another source of overpressure originates from clay diagenesis. The transformation of smectite to illite results in the molecular rearrangement of the clay structural tetrahedrals, which in turn, induces changes in the cation exchange capacity that then elicits the release of a large amount of formerly bound water. This expulsion of bound water has the potential to reduce the clay volume by up to 30% (Eslinger and Pevear, 1988). This results in both a pore fluid volume increase and a pore size decrease as the compaction characteristics change with the formation of illite. If this fluid is not able to escape the matrix pore structure, it will result in an overpressured situation. The Delaware Basin is old enough that areas below the Bone Spring Lime are nearly complete in their transition from smectite to illite. However, as pointed out be Lee and Williams (2000), even the most robust seals from shales are not capable of holding an instant of overpressure for over 200 million years. Therefore, it is very reasonable to assert that some of the original instances of overpressure in the Delaware Basin may have been the result of clay diagenesis in the Delaware Basin. However, an additional overpressure mechanism should be considered to explain the currently elevated and abnormal pressures.

1.3.3. Fluid Movement

In permeable formations, fluid movement can result in abnormal pressures. The hydraulic head from an elevated water table, possibly in a mountainous region, can lead to a formation pressure near the hydrostatic pressure as calculated from the height of the water table rather than the formation depth. In order for this to occur however, the water must be in good pressure communication with the formation in question and the overlaying formations must form adequate seals.

Tall vertical hydrocarbon fluid columns can result in overpressured regions. Oil and gas both have lower densities and therefore lower pressure gradients than formation water. Therefore, the pressure profile would show that the formation sections in the oil and gas portion of the column would be above hydrostatic pressure and classified as overpressured. This situation is generally seen in basins with thick permeable rock layers that are in good pressure communication through the height of the fluid column.

In addition to matrix porosity, fractures and faults provide a common mode of transferring high pressure from a deep formation to a shallower lower pressured formation at the end of the fracture. This follows the principle that fluids tend to travel from areas of high to low pressure and that hydrocarbons are buoyant relative to in-situ brines.

1.4 Estimating Formation Pressures with Well Logs

Hottmann and Johnson (1965) were the first to develop a method to identify and calculate overpressure from well logs. Their method for pore pressure estimation from well log data was based on the principles of compaction laid out by Hubbert and Rubey

(1959), "for a shale to compact, fluids must be removed. Sands, which are highly permeable media, act as avenues of fluid escape. These sands may be thought of as a pipeline. The near-absence of sands in thick shales reduces the rate of fluid removal from these shales in comparison with thinner shales sandwiched between sands…In such shale intervals, the permeability is quite small and fluid removal is restricted; thus the shale fluid pressure will be large for a given burial depth."

Hottmann and Johnson and later Eaton developed their models using log data in the Texas-Louisiana Gulf Coast. That region primarily deals with overpressure from undercompaction, where overburden pressure is a primary actor. Hottmann and Johnson state that "these techniques are limited to areas in which the generation of overpressures is primarily the result of compaction processes in response to the stress of overburden." Their techniques have developed a proven track record for accurately estimating pore pressures in suitable basins.

This project expands on Ben Eaton's equation for formation pressure prediction using well log information (Eaton 1975). Building off the trends recognized by Hottmann and Johnson (Hottmann and Johnson 1965), Eaton determined that sonic logs can be used to predict pore pressures with the following equation:

$$\frac{\mathrm{P}}{\mathrm{D}} = \frac{P_{OB}}{\mathrm{D}} - \left(\frac{P_{OB}}{\mathrm{D}} - \frac{\mathrm{P_{Hydro}}}{\mathrm{D}}\right)\left(\frac{\Delta \mathrm{T_{norm}}}{\Delta \mathrm{T_{ob}}}\right)^{3.0} \tag{1.7}$$

where P represents pore pressure in psi, D represents depth in feet, P_{OB} represents overburden pressure in psi, P_{Hydro} represents normal hydrostatic pressure in psi, ΔT_{norm} represents the expected sonic compression wave response at the given depth as found from a normal compaction trend line in μsec/ft, and ΔT_{ob} represents the observed sonic response at the given depth in μsec/ft.

Adjusting Eaton's equation to solve for pressure magnitude rather than pressure gradient produces the equation:

$$P = P_{OB} - (P_{OB} - P_{Hydro})(\frac{\Delta T_{norm}}{\Delta T_{ob}})^{3.0} \tag{1.8}$$

These equations are rooted in the fact that decreasing porosity as a function of depth in normally pressured formations can be seen in sonic logs. The observed sonic response, ΔT_{ob}, should decrease with depth as porosity decreases. This gradual reduction over the length of the well is called the Normal Compaction Trend (NCT). If a layer in the formation is overpressured, then ΔT_{ob} should increase. In other words, if the porosity of a given formation lithology is higher than what would be expected based on the NCT, then it is generally the result of higher pressure. Thus, the departure from the NCT line is an indication of overpressure. This suggests that the formation pressure can be estimated from the sonic log's degree of departure from NCT. It is important to note, however, that the sonic response is predominately affected by lithology and porosity. Therefore, it should be expected that the accuracy of the pressure estimation will be affected by the lithology of the formation under investigation.

Figure 1.7 from Schlumberger's Log Interpretation Charts manual (2013) illustrates the relationship between porosity and the sonic response for three common lithologies: dolomite, limestone, and quartz sandstone. The red lines are empirically derived values. The solid blue lines are the weighted average of known matrix velocities. The B_{cp} is a lack of compaction correction applied to the matrix velocity for an unconsolidated sand. Knowing that porosity traditionally decreases with depth, the expected decrease in ΔT can be seen by following the red lines to the bottom left of the graph as the porosity value decreases. **Table 1.1** lists the matrix velocities and sonic transit times of the same three mineral matrices. **Table 1.2** lists the fluid velocities and sonic transit times of reservoir fluids and air.

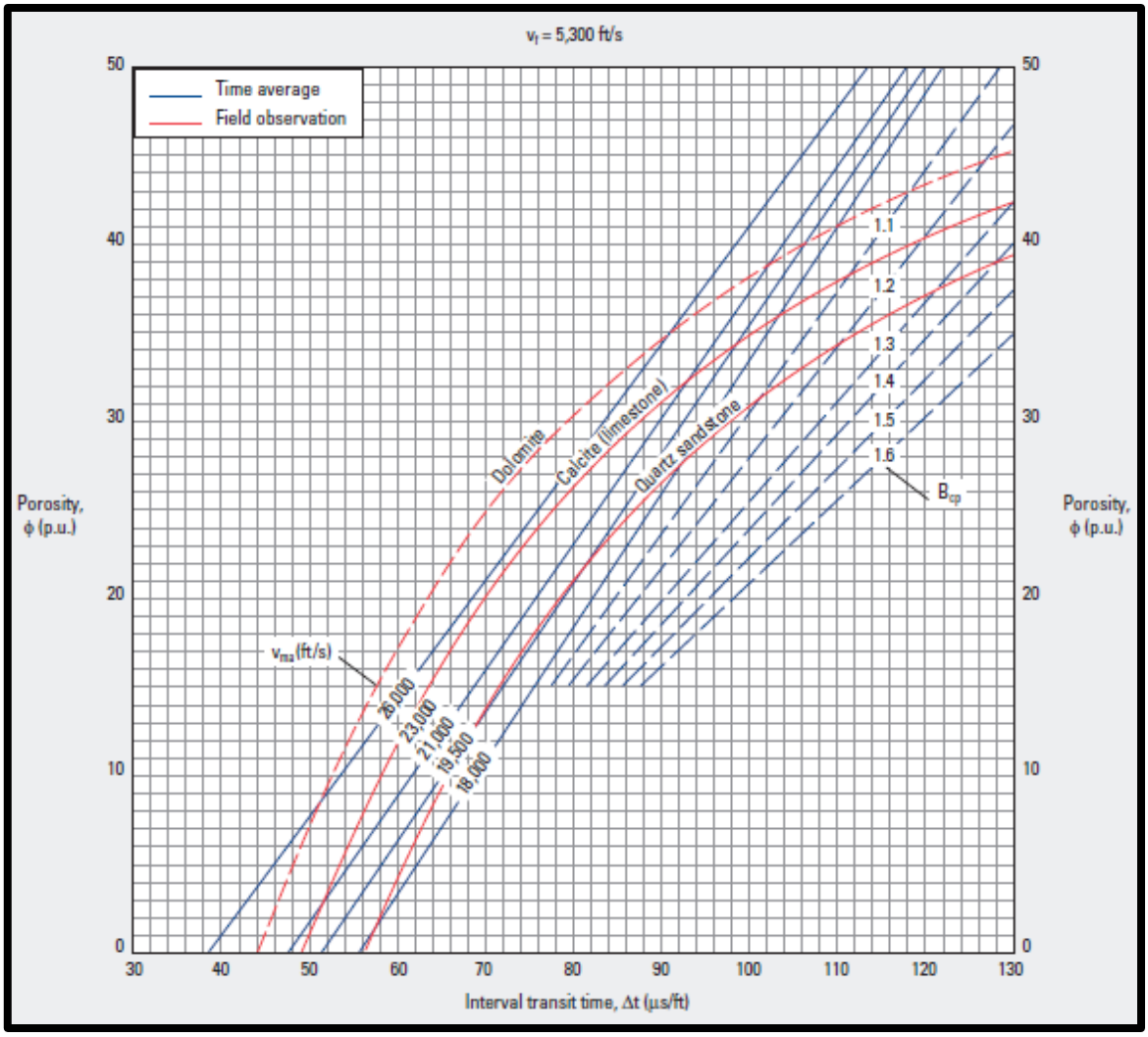

Figure 1.7. Schlumberger's sonic transit time to porosity conversion chart (Schlumberger, 2013)

Lithology	v_{ma} (ft/s)	Δt_{ma} (μs/ft)
Sandstone	18,000-19,500	55.5-51.3
Limestone	21,000-23,000	47.6-43.5
Dolomite	23,000-26,000	43.5-38.5

Table 1.1. Mineral matrix velocities and matrix transit times (Schlumberger, 2013)

Fluid	v_{fluid} (ft/s)	Δt_{fluid} (µs/ft)
Water	4,800	208
Oil	4,200	238
Methane	1,500	667
Air	1,100	909

Table 1.2. Fluid velocities and transit times (Timur, 1987)

2. METHODOLOGY

In order to employ the discussed methods and knowledge, an area to study must be selected. The region should have adequate geographic coverage of wells with sonic logs. After selecting a region, the process of preparing the data for investigation begins. While the sonic log is the decisive component of the investigation, additional log curves are needed to enable lithology identification. The general process for the study follows **Table 2.1.**

2.1 Temperature Gradient Development

After selecting the wells, a temperature gradient must be developed for the area. The temperature gradient is important because in addition to other corrections, the neutron porosity log requires an environmental correction for temperature. The most readily available method for formation temperature can be found in the header information of most well logs. Unless prior work on formation temperatures in the basin says otherwise, it is generally assumed that the maximum recorded temperature occurs at the bottom depth of the well. Consequently, both the depth and temperature are usually listed in the well log header information. The recorded temperature may not accurately reflect the true formation temperature since it is affected by the borehole mud, which may not have had adequate time to reach thermal equilibrium with the formation but it is usually the best available temperature estimate. As temperature does not stay constant from the bottom of the well to the surface, a gradient must be established in order to correct the neutron curve through the depth of the well.

Task	Notes
Basin Selection	Identify area of interest
Basin Division	Divide the area into sub areas based on geography and geology.
Well Selection	Select wells based on geographic distribution, depth, and available logs. Sonic, gamma ray, neutron porosity, bulk density logs are mandatory. A photoelectric log is preferred.
Temperature Gradient Development	Develop a temperature gradient to correct the neutron porosity curve based on the calculated average surface temperatures and bottom hole temperature.
Environmental Corrections	Apply appropriate environmental corrections to the gamma ray, neutron porosity, bulk density, and photoelectric log.
Verify Sonic Curve Data	Verify the sonic data validity based on the histogram data distribution and a map of average ΔT value Isolated to most homogeneous formation interval across all wells. Compare wells from each sub-area against each other.
Generate Maturity=f(Depth) regression lines	USGS Delaware Basin study used in this project
Map Maturity Regression Lines	Note any drastic changes to rate of maturation across the basin
TOC Identification	Use Passey's ΔLogR to identify TOC and organic rich shales.
Model Shallow Overburden Pressures	If current project well set does not have adequate bulk density data then find new wells with which to model shallow overburden pressure.
Develop Shale NCT	Isolate kerogen free shales on depth vs ΔT cross plots
Develop Sand NCT	Isolate kerogen free sands on depth vs ΔT cross plots
Map NCT Slopes	Map slopes to verify general agreement and smooth gradation
Calculate Pore Pressures	Use Eaton's equation to calculate pore pressure based on sand and shale NCT lines
Verify Pore Pressures	Calculate initial reservoir pressure based on flowback data, managed pressure drilling data, and DSTs. Compare the validation pressures to the estimated pressure from Eaton's equation.
Compare Sand vs Shale Estimated Pressures	The difference in the estimated pressures may indicate the formation's degree of coupling
Extrapolate maturity function to project wells	Apply kerogen maturity as a function of depth to each well in the project
Compare Overpressure to Maturity	Investigate correlation between maturity and over-pressured regions
	Well Set 1-Project Wells
	Well Set 2-Shallow Density Wells
	Well Set 3-TOC Maturity Wells

Table 2.1. Methodology overview

A multitude of factors can contribute to the development of a non-linear temperature gradient, to include formation thermal conductivity, fluid flow, and tectonics. But, for the purposes of environmental corrections to neutron logs, linear temperature gradients are generally acceptable. The second temperature and depth data points can be found by assuming that the temperature will be near the yearly average surface temperature at a depth very near the surface.

2.2 Environmentally Correcting Logs

While the study's pressure estimations are derived from the sonic log, many other logs are used to help filter data, identify lithology, estimate the quantity and location of organic material, and develop a better understanding of the formations. In addition to the sonic log, the gamma ray, caliper, deep resistivity, neutron porosity, bulk density, and photoelectric logs are utilized. Before any analysis can be performed, the well logs must be corrected to account for the effects of the borehole environment. Most modern day log analysis programs automate this process based on the specifications and charts provided by the service company that logged the well. The required input data to correct each log is generally found in the log header. For example, the software suite Interactive Petrophysics by LR Senergy corrects the Schlumberger gamma ray log for the borehole size effect based on the caliper readings, eccentered vs. centered tool positioning, mud type, mud weight, tool diameter, and standoff.

2.3 Mapping Kerogen Maturation

Vitrinite reflectance (Ro) is the most widely used method to measure kerogen maturity. Ro measurements can be taken from core samples or cuttings. For a basin

wide study, acquiring this maturity data can prove to be problematic. Many basins have public studies which present samples from across the area. E&P companies may have their own in house data from wells they have drilled and some companies may join a consortium with other operators to share data. But, error can be introduced if the sources are intermixed as quality controls and measurement standards may not be unified across all sources. For wells with multiple Ro measurements at varying depths, a trend line can be fit to the data so that Ro is a function of depth. Linear or logarithmic regression trends are usually acceptable for early modeling until a more definitive relationship can be established with more thorough sampling. Developing regression lines for multiple wells in the area allows for the creation of maps to sample the depths of the maturity levels to any location on the map. Thus mapping the regression lines allows for each well in the pressure study to be fit with a linear Ro=f(depth) curve.

2.4 Estimation of TOC using Passey's ΔLogR Method

Mapping the kerogen maturation in the previous step allows for a maturity estimation at any depth for any well in the study area. But, substantial TOC (percent weight of total organic carbon) is not uniformly present throughout all the formations. Therefore, Passey's ΔLogR (Passey et. al, 1990) technique is employed to estimate the TOC through the depth of the well. Multiple methods have been developed to estimate TOC using well logs, but Passey's method is generally the most widely accepted and has become an industry standard. The CARBOLOG (Carpentier et al. 1991), Schmoker (Schmoker, 1979), Western Canadian (Issler et al., 2002), and Passey's method all work based on the principle that the sonic, bulk density, and neutron porosity curves cannot distinguish TOC

from porosity. The organic matter registers as a high ΔT for the sonic tool, low density relative to formation bulk density for the life of the kerogen as read by the bulk density tool, and has a high hydrogen content as read by the neutron porosity tool. Each of these effects are similar to what the respective tools would see if they were measuring brine filled porous rock.

Passey's ΔLogR method (Passey et al. 1990) relies on the observation that by scaling and overlaying each porosity curve on top of a logarithmically plotted resistivity curve, the measured porosity due to TOC could be separated from the actual formation porosity, as shown in **Figure 2.1**. The organic matter has a lower conductivity compared to the formation water in the porous rock. So, a registered porosity reading with elevated resistivity can be used to identify the intervals containing the organic matter. TOC weight percent is a function of the separation (the Δ) between the overlaid porosity curve and the resistivity curve (the LogR).

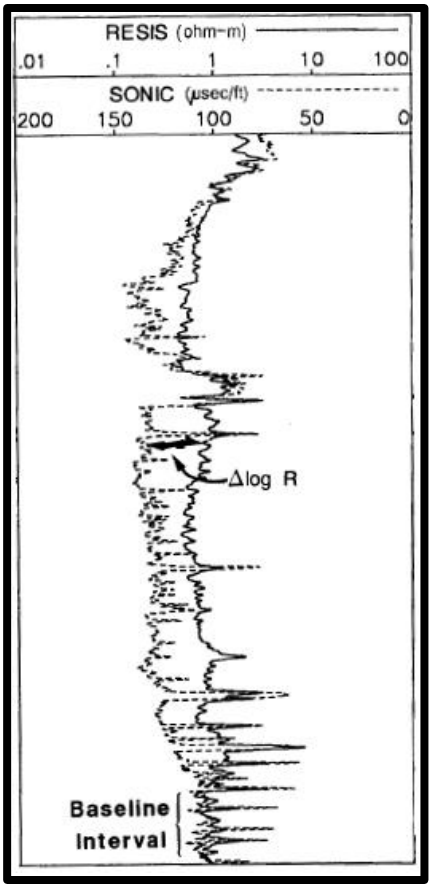

Figure 2.1. Visualizing Passey's ΔLogR overlay using sonic and resistivity logs, from Passey et al. (1990)

In Passey's method (Passey et al. 1990), kerogen maturity is measured based on the Level of Organic Metamorphism (LOM) scale, which was originally developed for coal ranking. LOM is more commonly referred to as level of maturity. Based on the early work of Vassoyevich et al. (1970), Hood et al. (1975) developed the plot in **Figure 2.2**, showing the hydrocarbon maturation stages as it relates to LOM progression. Since both Ro and LOM represent a measurement of maturity, it is convenient to have a conversion between the two. **Figure 2.3** shows the relationship between LOM and Ro using a 6^{th} order

polynomial that is fit to the data points. The resulting polynomial equation is shown as **Equation 2.1**. The polynomial fit was judged to be the best overall fit for the data, as highlighted by **Figure 2.4.** Exponential and power equations do not match the shape of the data and the logarithmic equation loses accuracy in the key range pertaining to the oil and early gas windows. The polynomial function gives very close agreement except in the extreme maturity case above Ro=4 and below Ro=5. Here there is some tendency for oscillation but the fit is still acceptable for studies primarily concerned with maturities much less than this window.

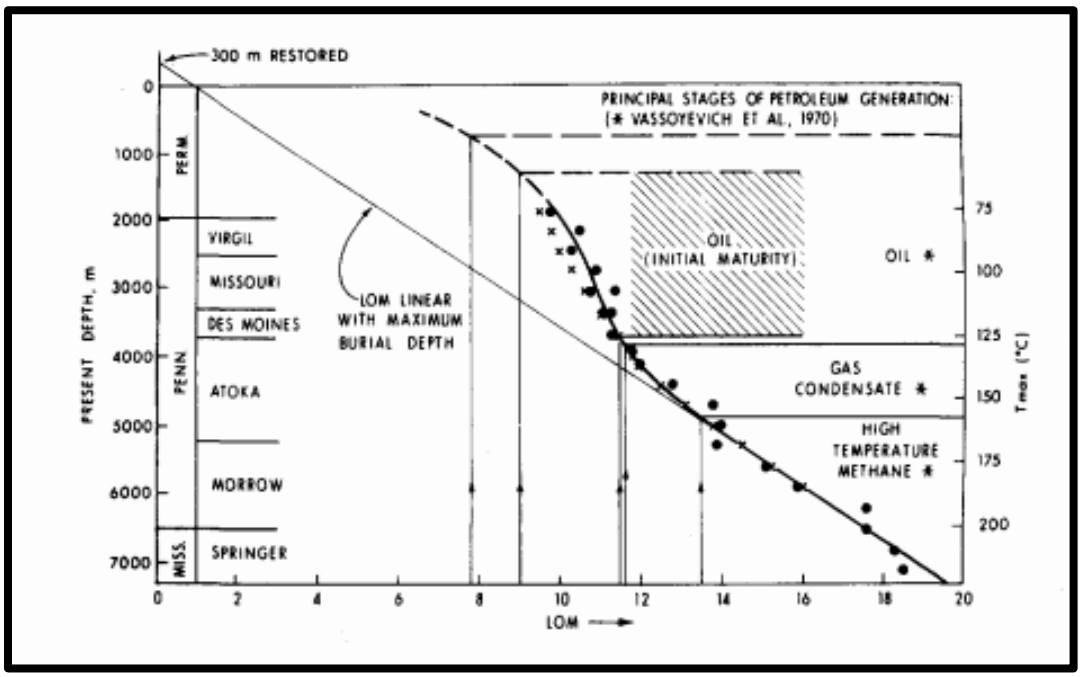

Figure 2.2. LOM and its relation to hydrocarbon development, from Hood et al. (1975)

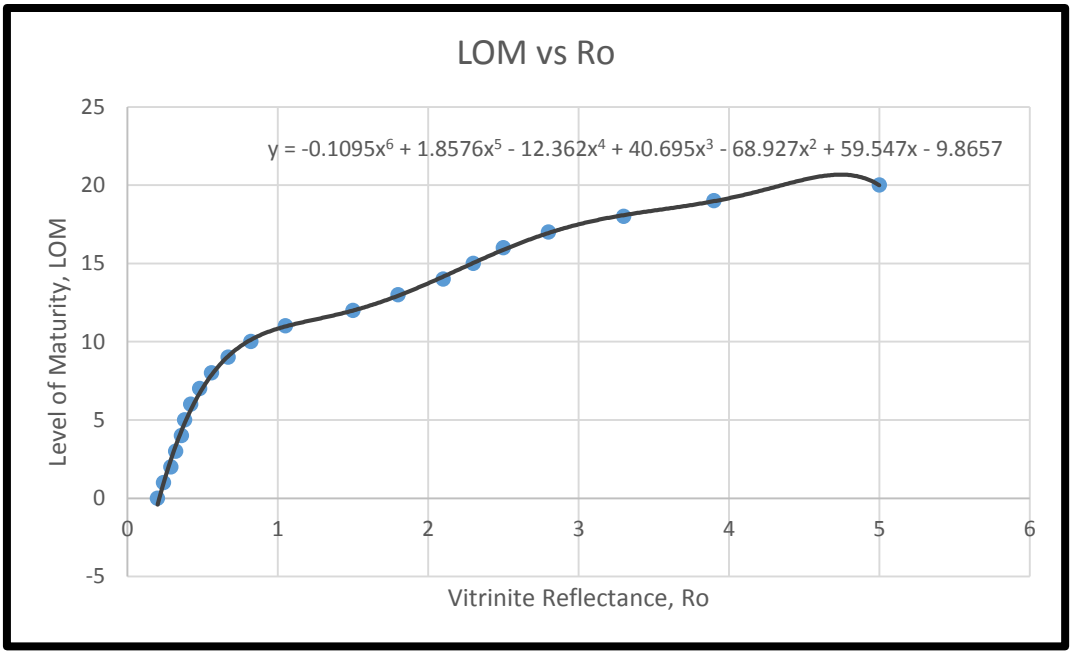

Figure 2.3. LOM vs Ro

The regression line used for the LOM vs Ro plot is the 6th order polynomial:

$$LOM = -0.1095Ro^6 + 1.8576Ro^5 - 12.362Ro^4 + 40.695Ro^3 - 68.927Ro^2 + 59.547Ro - 9.8657 \quad (2.1)$$

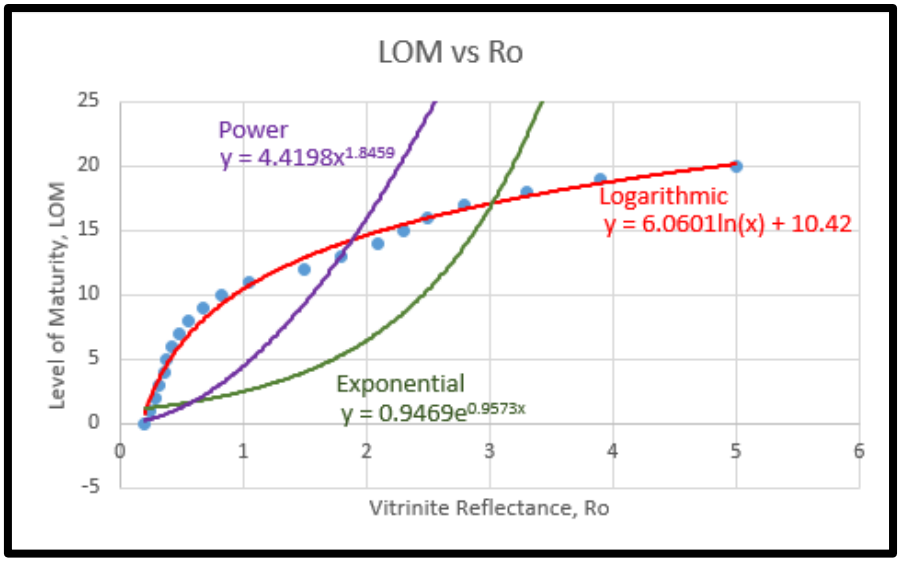

Figure 2.4. LOM vs Ro with alternate regression lines

Based on the ΔLogR measurement form the Passey's log overlays and the estimated LOM, TOC can be found by using the chart shown in **Figure 2.5.**

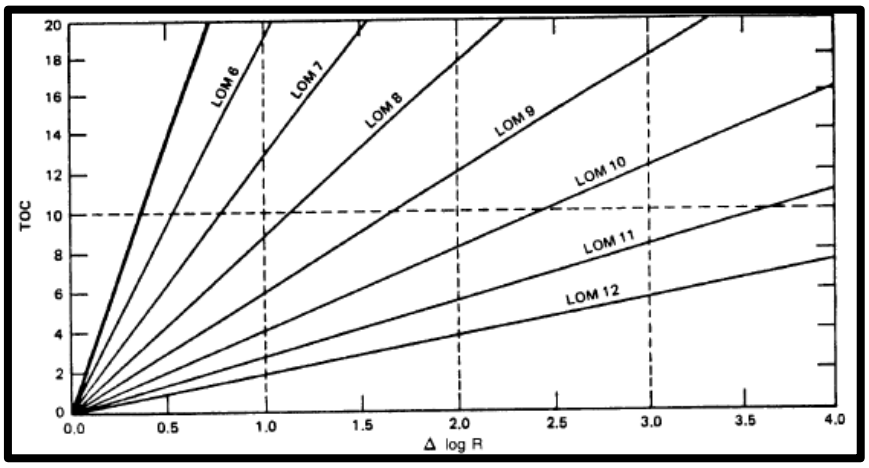

Figure 2.5. Determining TOC wt% from ΔLogR and LOM

Figure used directly from Passey et al. (1990). The y-axis TOC is the TOC wt%. Starting on the x-axis with the ΔLogR from the log overlays, users move vertically to the estimated LOM line and then horizontally across for the TOC wt%.

Passey, et al. acknowledged the fact that all resource shales contain some residual TOC. His study accepted the common assumption that a TOC of 0.8 wt% was a generally fair baseline for what should be considered as a value that is reasonably close to zero TOC. Passey accounts for the residual TOC in his empirically derived equation:

$$TOC = (\Delta \log R) \times 10^{(2.297 - 0.1688 \times LOM)} \tag{2.2}$$

Passey empirically derived corresponding equations for the above relationship for each of the three porosity measurements.

$$\Delta \log R_{Neu} = \log_{10}\left(\frac{R}{R_{baseline}}\right) + 4.0 \times (\phi \mathrm{N} - \phi \mathrm{N}_{baseline}) \tag{2.3}$$

$$\Delta \log R_{Den} = \log_{10}\left(\frac{R}{R_{baseline}}\right) + 2.5 \times (\rho_b - \rho_{baseline}) \tag{2.4}$$

$$\Delta \log R_{Sonic} = \log_{10}\left(\frac{R}{R_{baseline}}\right) + 0.02 \times (\Delta \mathrm{T}_{ob} - \Delta T_{baseline}) \tag{2.5}$$

where ϕ_N, ρ_b, and ΔT are the readings from the respective porosity curves. The baseline subscript designates the respective value in the baseline interval. The baseline interval is chosen as a layer of significant depth that is a non-source rock and fine grained.

Using the fact that sonic curves, the decisive curve in the pressure study, are influenced by the presence of TOC as demonstrated by Passey above, applying the ΔLogR technique will enable the identification and elimination of TOC affected data when constructing the normal compaction trend lines.

2.5 Developing Normal Compaction Trend Using Sonic Data

Implementing a similar model as Hottmann, Johnson, and Eaton into the Delaware Basin requires adjusting their original methodology because the Delaware is characteristically different from the Gulf Coast regions where the models were originally developed to be used. The Delaware is much older than the Tertiary Gulf Coast Basin. As such, the shales are more mature and nearly complete in their smectite to illite transformation and almost fully compacted. And, much of the formations of interest in the Delaware Basin are characterized by thin interbed sand and shale sequences. These sequences are often orders of magnitude below the resolution of conventional logging tools and can be much less than an inch, often only a few grains of sand thick. Additionally, the deposited kerogen in the Delaware Basin formations has progressed further in the maturation process than the kerogen in the Gulf Coast. Given the relatively low permeability in parts of the lower Bone Spring Sands and Wolfcamp, the generated hydrocarbons may tend to be much less moveable than the hydrocarbons in the zones of interest in the Gulf Coast. These Gulf Coast zones are composed of thick, predominately sand layers in which overpressure was largely the result of undercompaction.

Hottmann, Johnson and Eaton outlined that sand is not traditionally used as a medium to estimate pressure from well logs. Due to its permeability, a layer of sand is able to

distribute overpressure. Sand's high permeability relative to shales allows for the pressures caused by hydrocarbon generation to distribute across the sand layer. As previously discussed, Lee and Williams (2000) showed in their pressures simulation study on the Delaware Basin that shales orders of magnitude thicker than what we see in in the basin and with a permeability set to near impossibly low limits cannot maintain an instance of overpressure for much over 200 million years, which is much younger than many of the shales of concern in the study. Thus, in order for overpressure to exist today, it must be continually supplied from additional sources. This pressure is supplied through hydrocarbon generation from the kerogen embedded in the shale.

In a departure from the traditional methods outlined by Hottmann, Johnson and Eaton, sand is also used in this study as a lithology in which to estimate pressure from well log data. A sand trend line is employed because the continuous pressure stemming from hydrocarbon generation is partially expelled into the thin layers of sand interbred with the shale layers. The pressure is trapped in the sand regions by the layers of shale surrounding it. The continual hydrocarbon generation process allows for the pressure maintenance that would otherwise dissipate over geologic time, as described by Lee and Williams (2000). In describing their methods to detect overpressured regions in shales, Hottmann and Johnson (1965) regard the sonic log to measure the "change in porosity with depth". This study frames this change as an expansion in pore volume. The shales see a small expansion of the volume occupied by the kerogen as the produced hydrocarbon presses outward and also from the increasing organic porosity resulting from kerogen's decay into hydrocarbon. Thus, deviation of the sonic ΔT from the normal sand trend is utilized as a

measure for formation pressure. The measured pressure is an estimate of the pressure trapped in the sand regions that is generated from the organic rich shales. Fundamentally, Eaton's equations for pressure estimation from well logs are not confined solely to shales and can thus be used for sands in this case.

The slope of the sand trend decreases at a smaller rate than the shale trend. This is primarily due to the structure of clay vs sand. Pore volume in sand will generally decrease by rearrangement in grain packing and grain destruction to some extent at very high overburden pressures. Pore space within the clay will decrease primarily through dewatering and packing. Given the proven utility of Eaton's pressure estimation method in shales, it is still employed in the study. But, the pressure calculated from the shale trend is postulated to be an indication of the pressure trapped in the organic pockets of the shales. The difference in the pressures may be an indication of how well coupled the formation is between the sand and shale layers.

The sand trend line works in the Delaware Basin as shown in **Figure 2.6.** Characteristically, the permeability of the sand dictates the sand layers should fall on the sand trend line. But, if they are interbed with shale layers above and below, then the pressure generated in the shales from hydrocarbon generation or undercompaction is trapped in the sand layers by the shales. This increases the sand ΔT response as shown in **Figure 2.6**. The layers in the diagram reflect the thicknesses commonly seen in the Delaware basin and can range from an inch to small fractions of an inch. The shale ΔT response reacts as described by Hottmann and Johnson as overpressure causes the

expansion of pore volume. The red and blue horizontal arrows represent the differences in the ΔT_{norm} and $\Delta T_{observed}$.

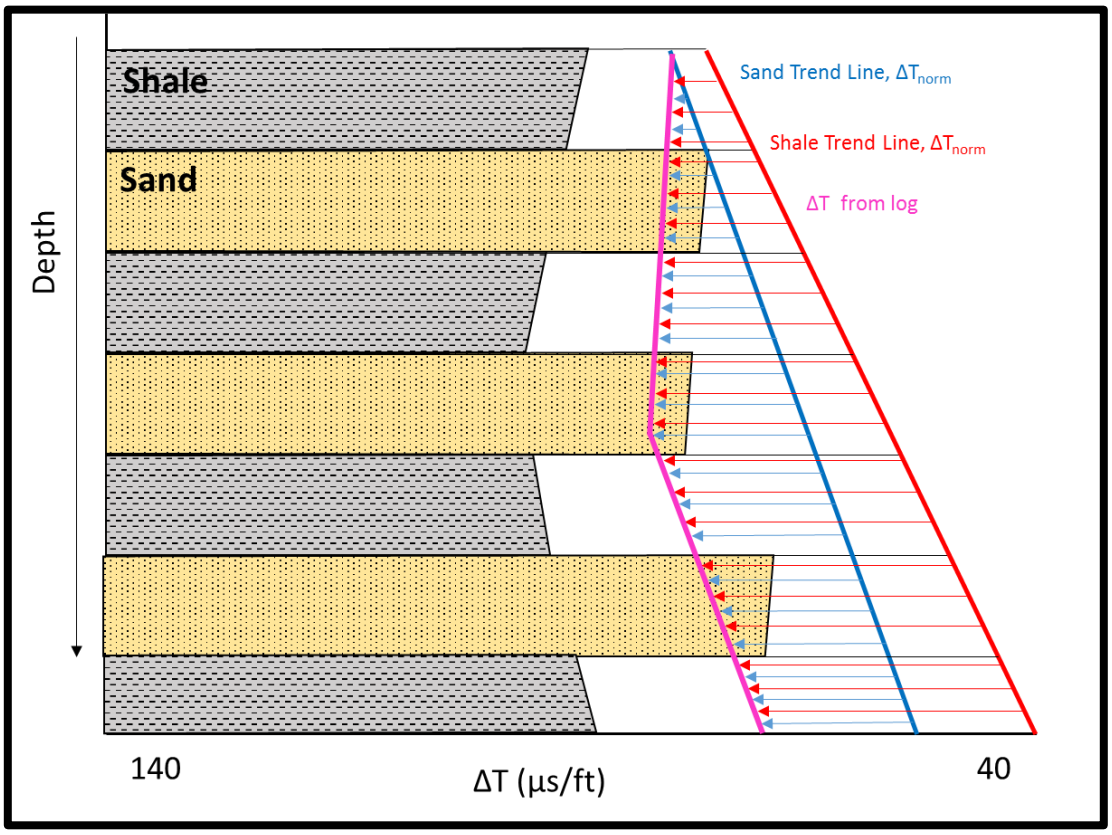

Figure 2.6. Diagram of sand and shale sonic response

Effective use of Eaton's equation for pore pressure prediction relies on accurate trend line development from the sonic curve on a depth vs ΔT (µs/ft) cross plot. However, normal compaction trend lines can be difficult to determine in a raw sonic log. Additionally, these trends are unique to each lithology. Porosity variations and the subsequent ΔT fluctuations among the different lithology types can obscure a NCT. But, meaningful pressure estimations can be achieved by isolating the NCT for a specific

lithology. The data points on the sonic log for the lithology under investigation can be isolated by applying constraints based on values from the other logs available for the well. For example, measured ΔT data points for shales can be separated from those of sands by constraining the depth vs ΔT cross plot to contain only the data points with a gamma ray value greater than 65 GAPI. Kerogen effects can be filtered out by eliminating the data points which contain TOC, as found from Passey's ΔLogR. Thus, shale formations influenced by TOC can readily be eliminated from consideration when constructing the NCT. This should be done because TOC in shale will affect the log response as kerogen maturation will increase the compressional wave travel time ΔT (μs/ft) above the normal response. Additionally, shale layers are primarily the areas of the formation capable of maintaining overpressure. This approach is most powerful in basins where shales are prolific enough that trends can be established without skipping significant portions of formations.

2.6 Overburden Pressures Estimation

Generally, the total overburden pressure gradient is assumed to be approximately 1 psi/ft. However, the overburden pressure gradient is not a constant. Its rate changes with depth because neither the formation composition nor its bulk density are constants. In his research on formation parting pressure prediction methods, Eaton (1969) outlined that the dynamic overburden can be estimated using bulk density logs. He determined that from the bulk density, the overburden gradient can be calculated with the equation:

$$\frac{P_{OB}}{D} = 0.433\rho_b$$

(2.6)

where P_{OB} is overburden in psi, D is depth in feet, and ρ_b is bulk density in g/cm^3.

Eaton's coefficient of 0.433 in **Equation 2.6** was used as the conversion factor to convert g/cm^3×depth (in feet) into psi. Bulk density logs are commonly plotted in units of g/cm^3. Recall that psi is lbf/in^2 (not lbm/in^2) so it is necessary to account for gravitational acceleration. The conversion is outlined below:

$$\frac{1g \times 1ft}{cm^3}\frac{1lbm}{453.592g}\frac{16.387cm^3}{1in^3}\frac{12in}{1ft}\frac{3.281ft}{1m}\frac{9.806m}{s^2}\frac{1lbf \times s^2}{1lbm}\frac{1}{32.174ft}$$

$$= 0.433\frac{lbf}{in^2}$$

(2.7)

Allowing the bulk density to vary with depth according to formation properties provides more accuracy for pressure calculations, as it is the driver behind the overburden pressure factor in Eaton's **Equation 1.8**.

2.7 Applying Eaton's Equation for Pore Pressure Estimation

After all the preparation, the data should now be ready to apply Eaton's equation to estimate the pore pressure of the formation. If the well does not have a bulk density curve starting near the surface, it can be estimated based on nearby wells that do have it or for rougher estimates, it can be assumed to be 1 psi/ft. Though Eaton's equation was written

for shales, it is applied to the sand trend line as well since the shales are heavily influencing the sands in the basin as discussed previously.

2.8 Validating Pressure Estimates with Available Data

Following the calculation of formation pressure estimates from sonic logs, it is vital to seek out real world data to validate the estimates. When selecting a field measurement method to validate the calculated pressure estimations, it is important to determine the vertical extent of the method. For instance, pressure validation estimates from MPD records should give a good estimation of pressure across the pay zone being drilled. Therefore the estimated pressure can be taken as the average calculated pressure from Eaton's equation across the same interval. For pressures from flowback data, the pressure validation will encompass the pressures across multiple intervals that may span several hundred feet, depending on the induced fracture height and orientation. The pressure estimation from logs should then encompass an average across a wider depth range than with MPD. DST data, on the other hand, is much more localized and depending on the tool, it may only convey the average pressure across a few foot wide interval. To validate pressure using DST data, it is best to use the gamma ray log to correlate the DST target to the project well depth.

3. APPLICATION

In this section, the methodology outlined in the previous chapter is applied to the Bone Spring and Wolfcamp formations in the Delaware Basin. This chapter serves as a proof of concept for what is anticipated to lead into a larger expansion of the study for an exploration and production company.

3.1 Study Layout

The study area is broken into five distinct and contiguous sub-areas of the basin as shown in **Figure 3.1**. For the study, the sub-areas are given the names Darby, Merrill, Rudder, Rogers, and Benning. The sub-areas are based on state and county lines and generally homogenous geological formation features.

The first step in the application phase was to run database searches of all wells in the basin. The minimum requirements for each well was that it must have had a gamma ray, sonic, deep resistivity, bulk density, and neutron porosity log. Wells with photoelectric logs were preferred but not deemed to be absolutely necessary. The logs also had to go through the Wolfcamp formation. Ultimately, 16 wells were selected for the study and will be referred to as the "project wells" henceforth. Well names were changed to protect the supporting company's data integrity. All plotted locations as shown on the map are meant to represent only general locations. In order to respect the integrity of the supporting company's data, the locations are only plotted as partially accurate. Spatial orientations and proximity to nearby wells are generally maintained. The wells provided a good distribution throughout the basin and across each sub-area. There is an absence of wells in the center portion of the study because much of that land is designated as a

potash mine. Historically, drilling has been very limited in the potash mine area and therefore logging data is sparse. An additional database search was executed for wells with shallow bulk density logs that were run in an open hole at depths near the surface. Shallow open hole logs are not common in the basin and six were found adequate for use in calculating the overburden pressure at shallow depths.

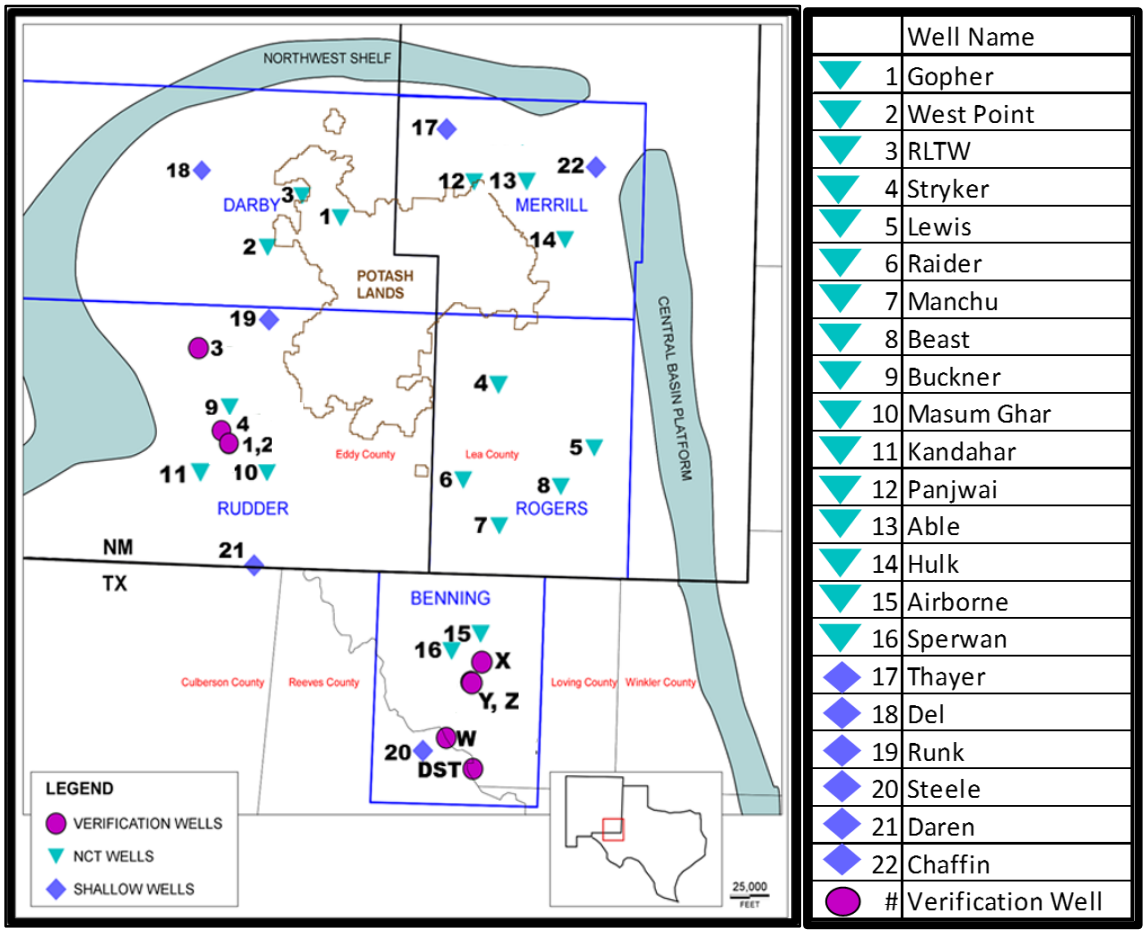

Figure 3.1. Delaware Basin study layout

Wells used for pressure estimations are represented with a teal triangle. Wells used to calculate shallow overburden pressure are represented with a purple diamond. Wells used to verify pressure estimates are represented with a pink circle.

3.2 Temperature Gradient Development

Prior to starting environmental corrections on the well logs, a temperature gradient was established in each sub-area of study. The gradient was specifically used to properly environmentally correct the neutron porosity curve. Unique gradients were necessary because the temperature gradient is not constant throughout the basin. Each log provides the maximum recorded bottom hole temperature (BHT) and the maximum depth. A second temperature is needed to generate the temperature gradient line. The log header provides the surface temperature but this is not the best option because it is obviously highly variable and dependent on the time of day, weather, and season. Instead, the approximate average surface temperature for the well's geographic location was used. It was assumed that the ground very near the surface would be near the area's average temperature. Climate data was used to find the average yearly temperature of the cities located within the study area. Next, a point in the center of each sub-area without a major city was selected and the elevation was recorded. Then using an air temperature gradient of 5.4°F/1,000ft, the sub-area's average temperature was calculated based on the elevation change from the city's average temperature to sub-area's center point. The average temperature for the point at the center of each sub-area was then assigned as the temperature at a depth of 0ft for the wells in the sub-area.

The temperature gradient per 100ft for each well was determined by

$$Temperature\ Gradient = \frac{Temp_{max} - Temp_{AreaAvg}}{Depth_{maximum}} * 100ft \tag{3.1}$$

The temperature gradients were averaged by sub-area. In order to allow for further rapid expansion of the study, the sub-area's average gradient was coded and assigned to all wells in the sub-area.

3.3 Environmentally Correcting Logs

All wells in the study were logged by Schlumberger. The Interactive Petrophysics environmental corrections module was used to apply the appropriate corrections through the entirety of all the log curves. Gamma ray logs were corrected based on tool position (eccentric vs centered), caliper readings (borehole corrections), mud weight, and mud type (barite or non-barite mud). The density and photoelectric logs were corrected based on caliper readings, mud weight, and the type of tool run (Compensated Formation Density vs. Lithodensity Tool). The neutron porosity tool was corrected for caliper readings, bit size, mud weight, temperature, borehole salinity, formation salinity, mud type (oil or barite mud), model of tool, and the input matrix. All the neutron logs were run with a limestone input matrix. If no borehole salinity was annotated on the log, it was estimated to be 100kppm NaCl equivalent. Formation salinity was estimated at 65kppm for all wells at the onset of the study. The deep resistivity and sonic logs were used raw.

The sonic data quality was verified by using a combination of the average ΔT in a homogenous formation and the ΔT distribution across an interval. Using the formation tops posted by resident geologists, the Bone Spring Lime formation (sometimes called the First Bone Spring Carbonate) was identified as the most homogeneous lithology section present in all the wells. Grouping the wells by sub-area, the average ΔT reading and ΔT distributions were compared. The average ΔT in the Bone Spring Lime was mapped as

shown in **Figure 3.2**. The mapped averages showed generally smooth gradation across the basin, where the values change in between 54 μsec/ft in the northern area of the study to 72 μsec/ft in the south. Histograms plotting the number samples, or ΔT, for discrete 2 μsec/ft sized bins were created to compare the logs' measurement distributions through the Bone Spring Lime. Good quality sonic logs should be expected to have generally similar distributions and similar centroids for wells grouped by sub-area. Drastically dissimilar sonic log histograms would indicate either a significant lithology change or a possible issue with the sonic measurements. The Bone Spring Lime ΔT histogram for the Darby Area is presented in **Figure 3.3**. Note the same general overall distribution of points. The spread of the ΔT count between each well can be attributed to the varying thickness of the Bone Spring Lime. Based on the smooth average gradation and uniform ΔT distribution for all wells, the sonic logs were judged to not need corrections.

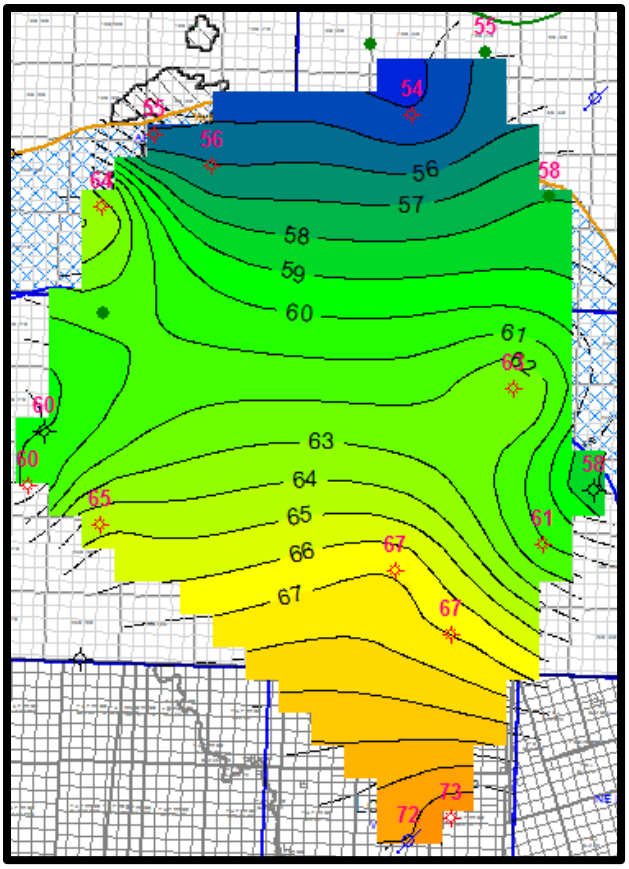

Figure 3.2. Average ΔT in the Bone Spring Lime interval

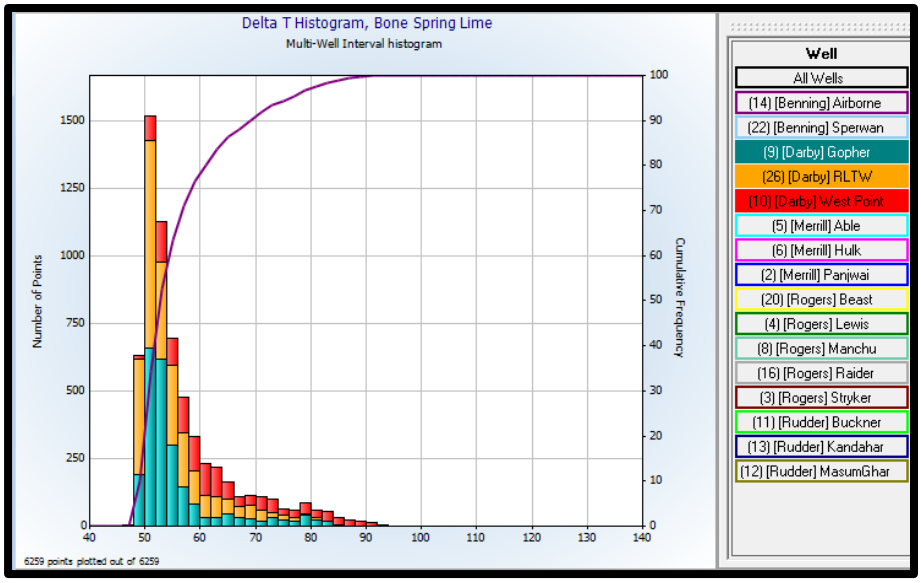

Figure 3.3. Sample histogram of ΔT values in the Bone Spring Lime, Darby Area

3.4 Mapping Kerogen Maturation

The vitrinite reflectance data from a United States Geological Survey (USGS) study of the Delaware Basin was utilized to develop regression equations and surfaces for Ro in the basin (Pawlewicz et al., 2005). The USGS study measured Ro values from samples taken from powdered cuttings in which zinc bromide was used to prepare the kerogen (Barker, 2015). The study area was overlaid on the USGS well layout map and the 32 USGS wells in or immediately around the study areas were selected as shown in **Figure 3.4**. These 32 wells were used to map Ro in study area.

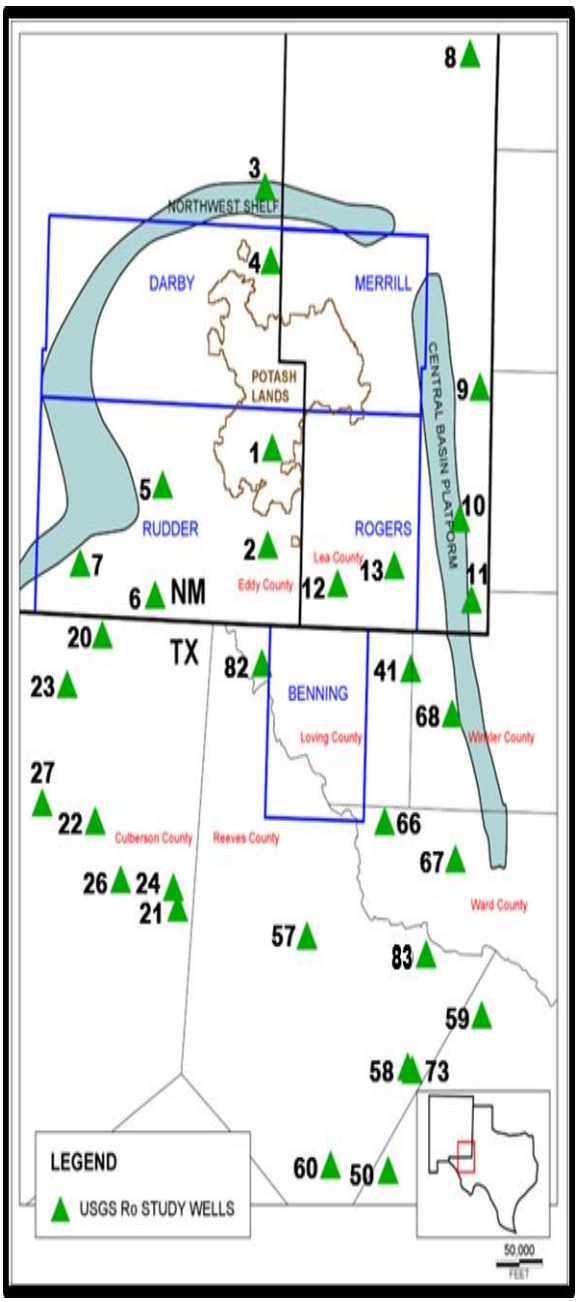

USGS Database Number	Well Name
1	JAMES RANCH UNIT 1
2	JF HARRISON FEDERAL 1
3	WEST B 27
4	GREENWOOD UNIT 1
5	STATE LSE K-2538 1
6	OWL DRAW UNIT 1
7	GOVERNMENT M 1
8	JL REED 1
9	NB BUNIN 1
10	MEXICO 2
11	FEDERAL-LEONARD B 1
12	RED HILLS UNIT 1
13	GULF-FEDERAL 1
20	EE POKORNY 1
21	GRISHAM-HUNTER-STAT 1
22	VELMA C ROUNSAVILLE 1
23	HOMER COWDEN A 1
24	GRISHAM-HUNTER-STAT 1
26	MARVIN R WEATHERBY 1
27	ROUNSAVILLE MVC 1
41	LINEBERRY EVELYN 1
50	KELLY STATE GAS UNI 1
57	MRS VL SHURTLEFF 1
58	WAPLES-PLATTER 1
59	HORRY L ETAL 3
60	TENNEY GERALD E 1
66	GREER-MCGINLEAS UNT 1
67	UNIVERSITY PYOTE UN 1
68	ROARK IC 1
73	WD #1Wilson
81	Calvert A #1
82	Lago Unit #1

Figure 3.4. Layout of wells used from USGS Study for Ro depths

The raw USGS Ro data was plotted for each well as % Ro vs Depth and any apparent data outliers were removed. **Figure 3.5** shows the combination of all the data points, colored coded by well and with outliers removed for each USGS well used in this study. Distinct linear and logarithmic trends were observed in the plot for each well. Next, a regression line was fit to each well's data as shown in **Table 3.1** and **Figure 3.5**. Each well's regression line's slope and intercept were surfaced over the map. The surfaced area encompassed the location of each well in the study, though the coverage across sub-areas Darby and Merrill is sparse and elicits a lesser degree of confidence in the accuracy of the extrapolated Ro trends. Using the Ro=f(depth) equation, slope and intercept values for all project wells were then interpolated from the USGS slope and intercept surfaces. Finally, the Ro values from the interpolated regression curve for each project well were then converted to a LOM curve using **Equation 2.1**.

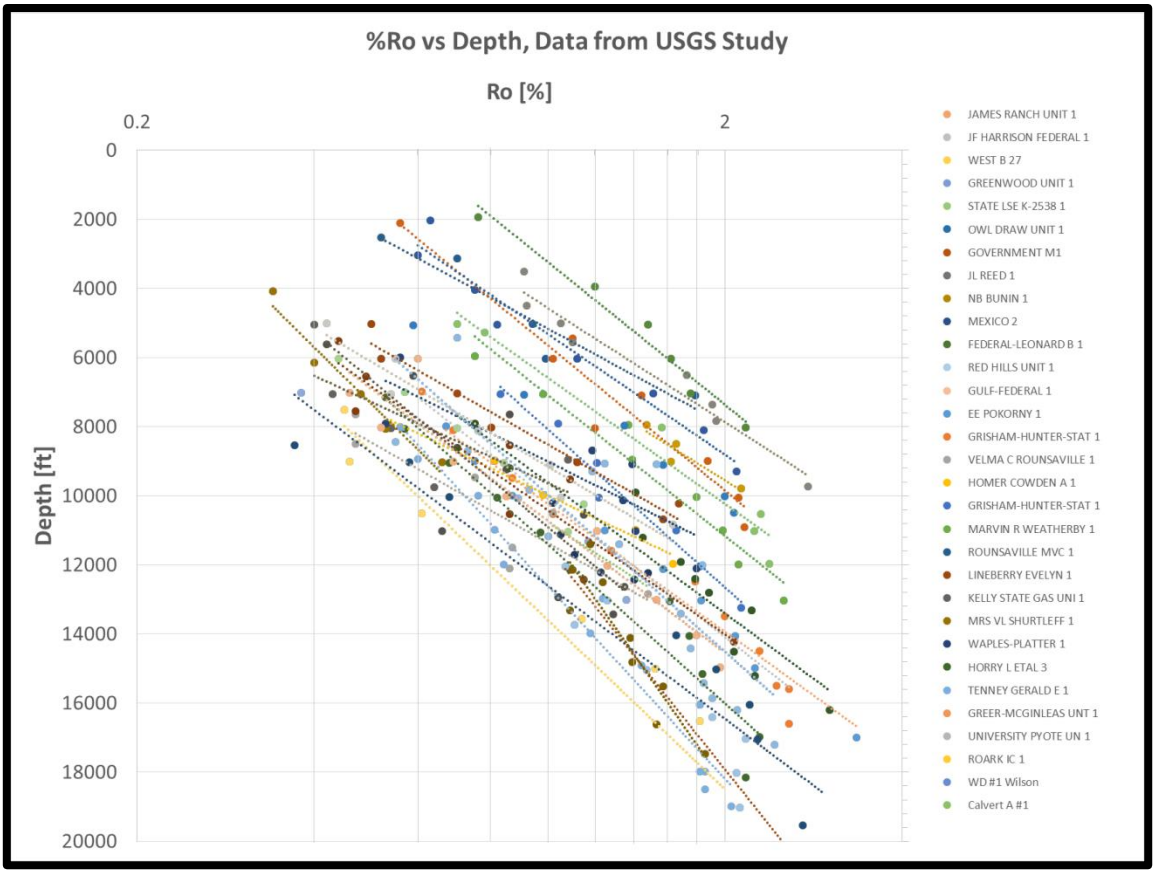

Figure 3.5. Ro vs Depth from USGS study wells with example well regression lines

API	USGS Database Number	Well Name	Regression Equation	R^2
30015047350000	1	JAMES RANCH UNIT 1	Ro=0.00028*Depth-1.881	0.96
30015047490000	2	JF HARRISON FEDERAL 1	Ro=0.00023*Depth-1.292	0.97
30015050740000	3	WEST B 27	Ro=0.00015*Depth-0.767	0.74
30015056140000	4	GREENWOOD UNIT 1	Ro=0.00028*Depth-1.707	0.98
30015103580000	5	STATE LSE K-2538 1	Ro=0.00021*Depth-0.639	0.96
30015107300000	6	OWL DRAW UNIT 1	Ro=0.00024*Depth-0.666	0.98
30015200340000	7	GOVERNMENT M 1	Ro=0.00023*Depth-0.095	0.82
30025051030000	8	JL REED 1	Ro=0.00022*Depth-0.764	0.92
30025079030000	9	NB BUNIN 1	Ro=0.00001*Depth-0.136	0.42
30025111230000	10	MEXICO 2	Ro=0.00006*Depth+0.056	0.91
30025119770000	11	FEDERAL-LEONARD B 1	Ro=0.00021*Depth-0.751	0.82
30025210360000	12	RED HILLS UNIT 1	Ro=0.00017*Depth-0.827	0.96
30025221530000	13	GULF-FEDERAL 1	Ro=0.00013*Depth-0.652	0.96
42109000330000	20	EE POKORNY 1	Ro=0.00025*Depth-0.478	0.98
42109001670000	21	GRISHAM-HUNTER-STAT 1	Ro=0.00028*Depth-0.965	0.97
42109002220000	22	VELMA C ROUNSAVILLE 1	Ro=0.00019*Depth-0.031	0.90
42109002440000	23	HOMER COWDEN A 1	Ro=0.00031*Depth-0.446	0.95
42109003160000	24	GRISHAM-HUNTER-STAT 1	Ro=0.00033*Depth-1.251	0.84
42109100520000	26	MARVIN R WEATHERBY 1	Ro=0.00022*Depth-0.064	0.93
42109104290000	27	ROUNSAVILLE MVC 1	Ro=0.00021*Depth0.339	0.98
42301101700000	41	LINEBERRY EVELYN 1	Ro=0.00016*Depth-0.869	0.92
42371003610000	50	KELLY STATE GAS UNI 1	Ro=0.00017*Depth-0.747	0.94
42329016490000	57	MRS VL SHURTLEFF 1	Ro=0.00018*Depth-0.611	0.86
42389102050000	58	WAPLES-PLATTER 1	Ro=0.00013*Depth-0.602	0.93
42389102340000	59	HORRY L ETAL 3	Ro=0.00016*Depth-0.779	0.99
42389104640000	60	TENNEY GERALD E 1	Ro=0.00014*Depth-0.433	0.95
42475107290000	66	GREER-MCGINLEAS UNT 1	Ro=0.00021*Depth-1.396	0.99
42475107860000	67	UNIVERSITY PYOTE UN 1	Ro=0.00016*Depth-0.629	0.84
42495102480000	68	ROARK IC 1	Ro=0.00009*Depth-0.013	0.69
42389104740000	73	WD #1Wilson	Ro=0.00011*Depth-0.1989	0.83
42371104790000	81	Calvert A #1	Ro=0.00018*Depth-0.936	0.68
42301300450000	82	Lago Unit #1	Ro=0.00025*Depth-1.315	0.93

Table 3.1. USGS Ro regression equations

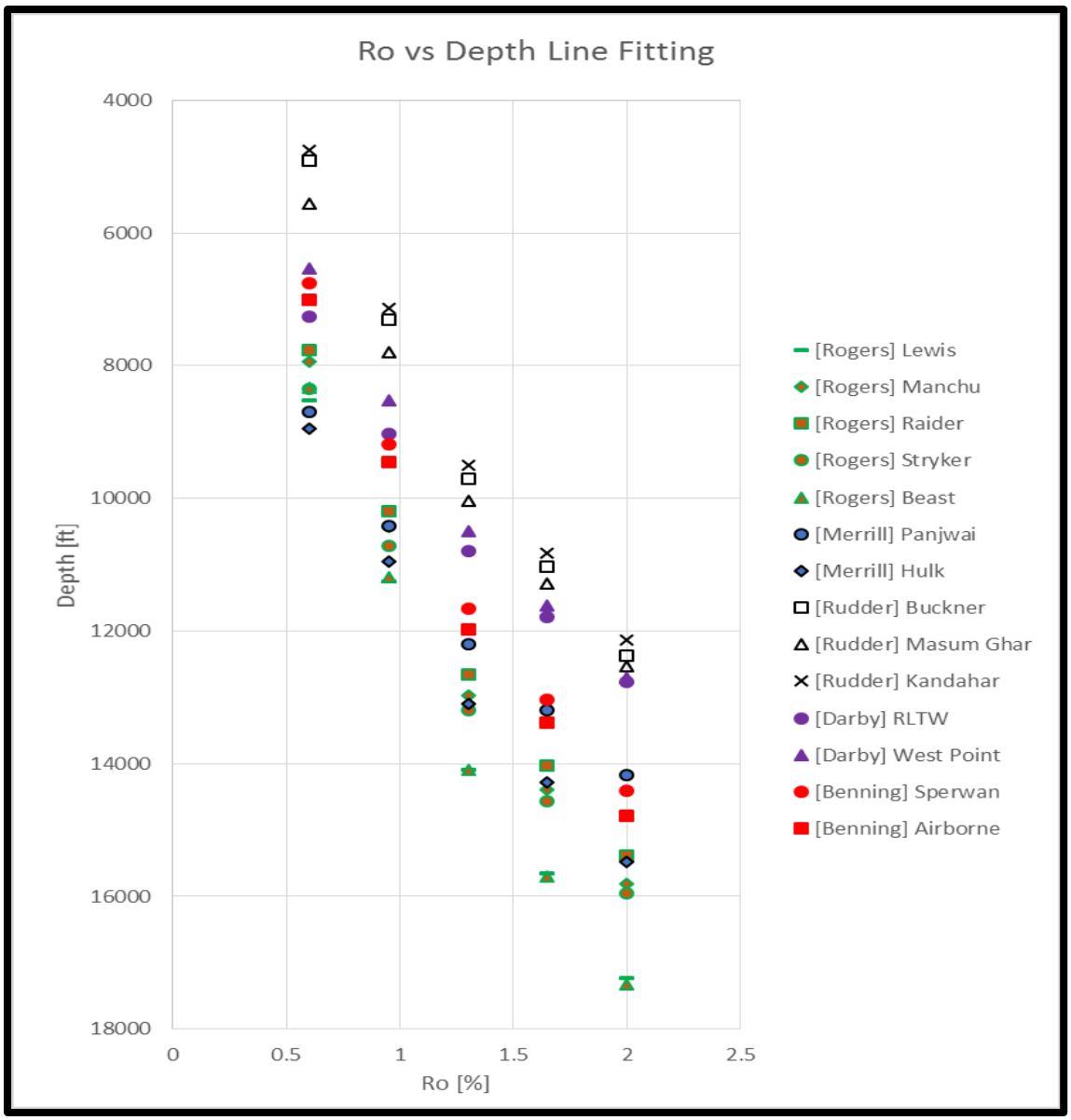

Figure 3.6. Plotted Ro benchmarks at corresponding depths from the generated Ro=f(depth) regression lines for each study well

3.5 Estimation of TOC using Passey's ΔLogR Method

TOC was calculated for each well using Passey's Delta Log R (ΔLogR) method using the sonic, bulk density, and neutron porosity curves. The TOC was taken as the average weight percent calculated from each of the three porosity curves. Initially, the LOM was assumed to be 10.5. This is not a precisely correct value, but during the initial portion of the study the purpose of TOC determination is merely qualitative; in that it serves to identify where the TOC is rather than identify how much TOC is in place. In this regard, LOM=10.5 is a highly conservative estimation and will underestimate the calculated amount of TOC present. This justification can be seen graphically by referring back to **Figure 2.5** and seeing that the chosen LOM serves only to impact the total amount of TOC present and not the binary present or not present attribute, which is the purpose of this step. The sand base line for each well in the study was determined to be in the Brushy Canyon and in some cases included the Bell Canyon as shown in the example in **Figure 3.7** at depths of 4,000-6,000ft.

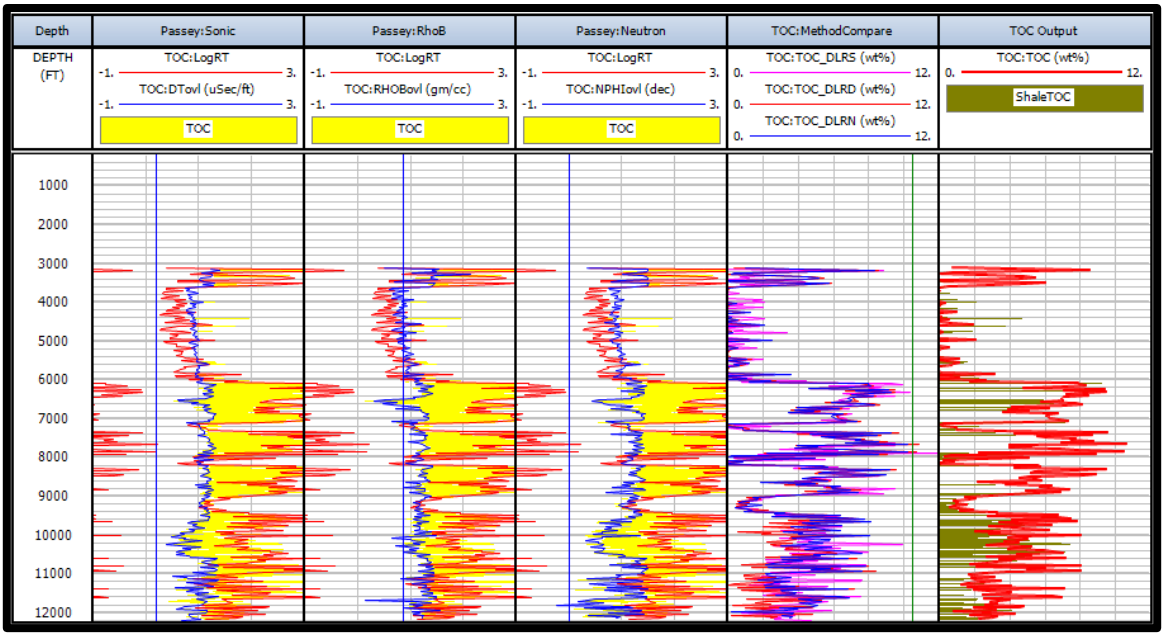

Figure 3.7. Sample ΔLogR Methodology for the West Point well

Figure 3.7 shows the work progression of the ΔLogR. Track 1 shows the depth. The sonic, bulk density, and neutron porosity overlays are shown in tracks 2, 3, and 4, respectively. The computed TOC from each method is shown in track 5. The curve TOC:TOC in track 6 shows the average TOC values through the depth of the well as calculated from the sonic, neutron, and density method. A constraint of gamma ray readings larger than 70 GAPI was applied to the TOC:TOC curve and all intervals meeting this constraint are colored in olive green and labeled ShaleTOC in track 6. This allows for the identification of organic rich shales. This is an important step because organic rich shales are postulated to distort the shale normal compaction trend line on the sonic curve.

3.6 Developing Normal Compaction Trends from Sonic Data

Next, the sonic logs for each well were plotted on a depth vs ΔT cross plot in order to develop the normal compaction trend lines for use in Eaton's equation. Throughout the project when using log curves to isolate specific lithologies, there was some variance in the range of values associated with specific lithologies. This variance comes from the aerial spread of the basin and the heterogeneities introduced from the depositional environment. Additionally, the timeline of the well logs span decades, multiple service companies, and various tool design versions. While environmental corrections should bring them into close alignment, each log is unique. Baseline shifting each log to bring them into agreement on specific lithology values could have been performed to standardize response ranges. But, recognizing the variability of these response ranges was deemed preferable. To isolate lithologies, first, all the carbonate and organic rich shales were removed from the plot. The carbonates were removed by eliminating all points that had a gamma ray reading less than 30-60 GAPI and a photoelectric factor (PEF) greater than 2.75-3.0 barns/electron (B/E). In cases where the lithology type was not readily apparent from only the gamma ray and PEF, an FDCCNL plot (also known as a bulk density vs neutron porosity cross plot) was used. The organic rich shales were cut from the plot by removing all points which corresponded with the previously discussed ShaleTOC values found with Passey's ΔLogR method (the olive green regions in **Figure 3.7**).

Operating with a depth vs ΔT cross plot free of carbonates and organic rich shales, the shale normal compaction trend was found first. Through trials it was found that the

most reliable and efficient method for isolating the shales was adjusting the gamma ray cut off to greater than 55-110 GAPI. It was found that the shale NCT generally began to develop in the Brushy Canyon. The depth vs ΔT cross plot for well Masum Ghar is shown with all data points present, minus the carbonate and organic rich shales in **Figure 3.8.** **Figure 3.9** shows the same well's cross plot with only organic free shales present with the compaction trend line fit to the data.

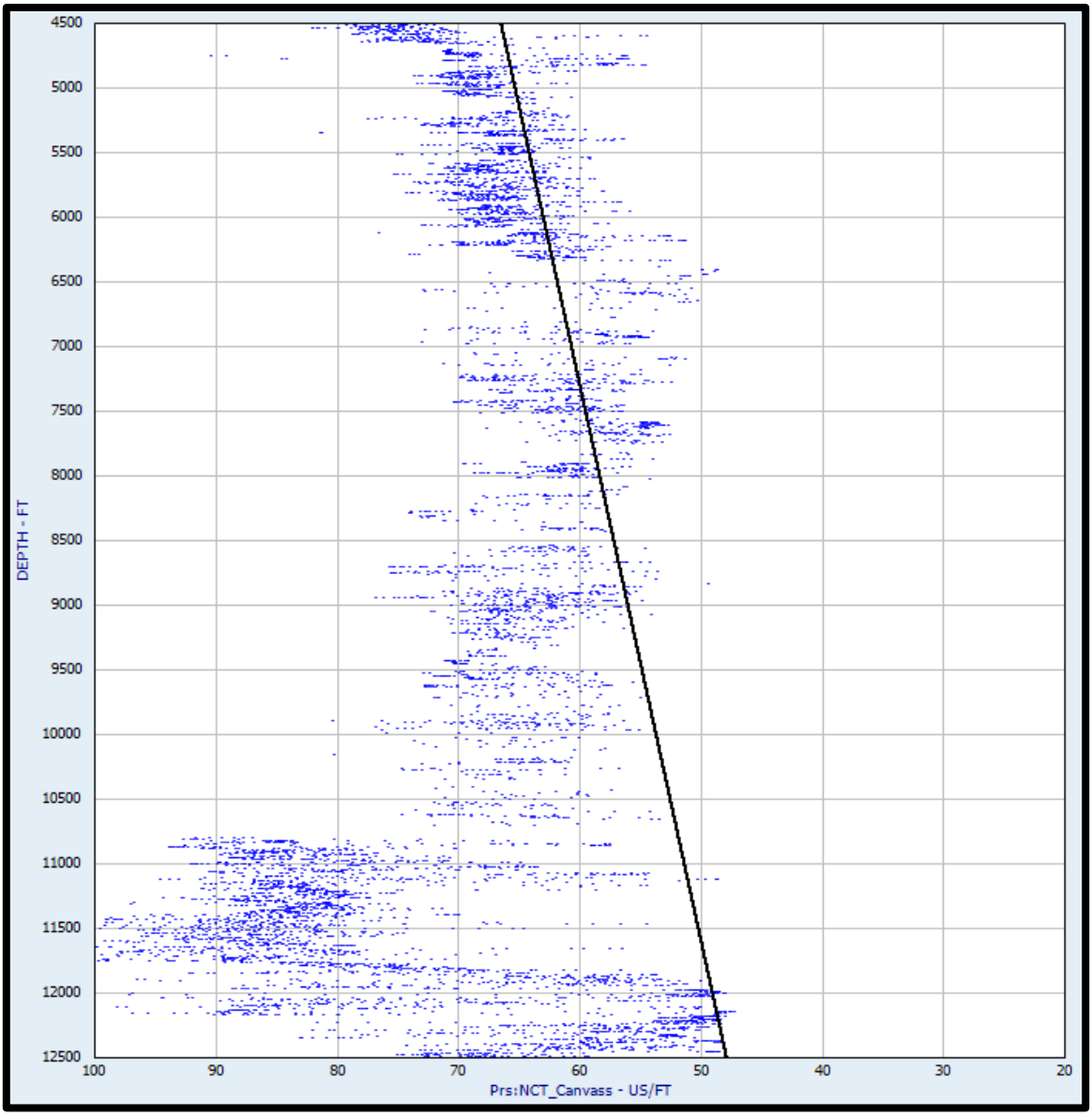

Figure 3.8. Well Masum Ghar's complete Depth vs ΔT data set, minus carbonate and organic rich shale, with the shale compaction trend line drawn in black

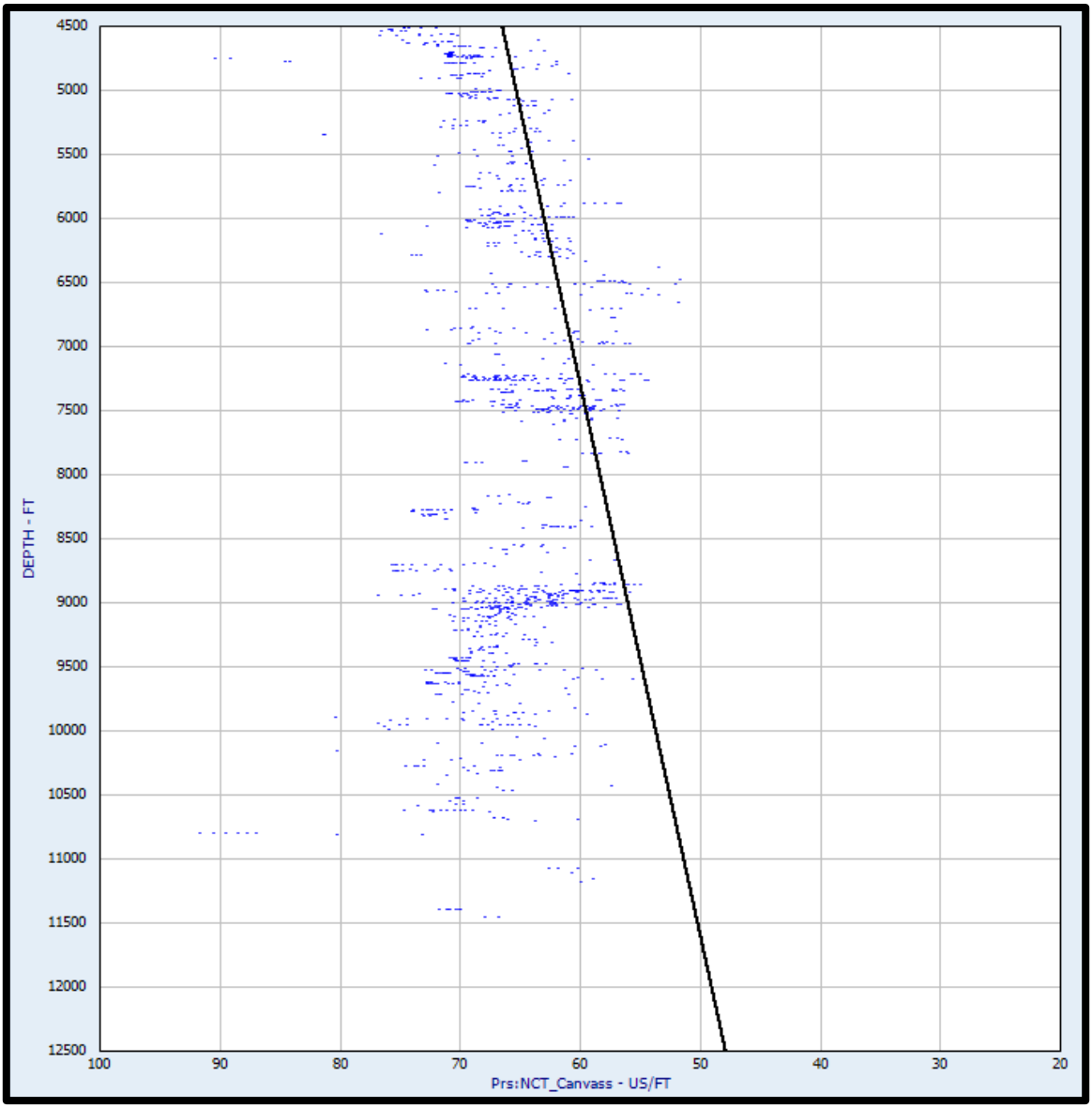

Figure 3.9. Well Masum Ghar's Depth vs ΔT Cross Plot, minus carbonate and organic rich shale, with a Gamma Ray discriminator applied to isolate TOC free shale regions

In addition to the shale compaction trend, a sand NCT was constructed on the Depth vs ΔT cross plot. The sand NCTs were developed using the same methodology employed for the shale NCT construction. First, the carbonates and organic rich shales were removed. Then, the remaining data was constrained to only points with a gamma ray reading less than 35-57.5 GAPI and a PEF reading less than 2.5-3.5 B/E. Similar to the shale trend, the sand trend generally becomes evident in the Brushy Canyon formation for the all the project wells. The isolated sand regions and trend line for well Masum Ghar are shown on the cross plot in **Figure 3.10**. In cases where the well did not have a PEF log curve, the bulk density, neutron porosity, and deep resistivity curves were used to isolate the lithologies.

Given the difference in atomic structure of shale and sand, different compaction trends are expected. Crystalline realignment and bound water expulsion both will contribute to the compaction trends in the shales. But, as sands lack the bound water component, their compaction and subsequent decreasing porosity will be a function of granular realignment and granular particle destruction with increasing overburden pressure. The rate of change of the compaction trend for sands will generally be less than that of shales.

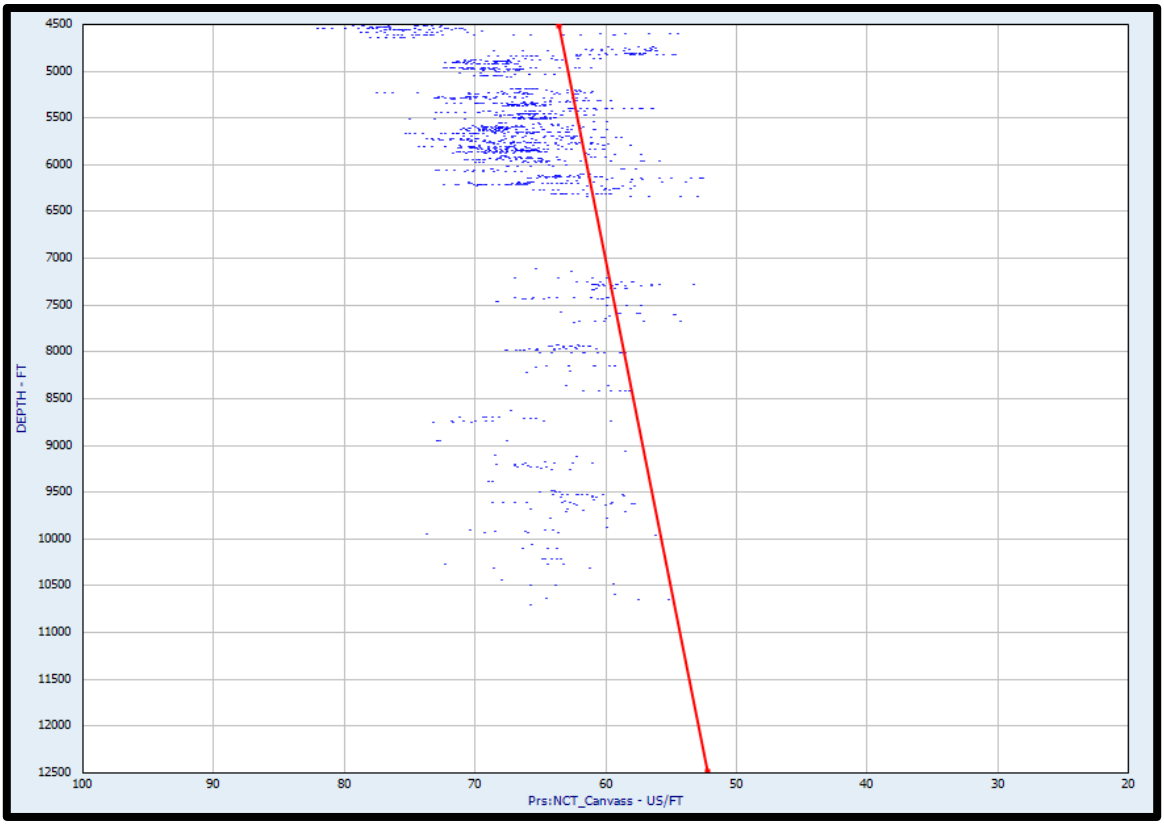

Figure 3.10. Well Masum Ghar's Depth vs ΔT Cross Plot, with discriminators applied to isolate sand regions

3.7 Calculating Overburden Pressures

In order to apply Eaton's equation, the overburden pressure had to be calculated for each well. Most wells in the basin do not have open hole logs approaching the surface depth. Therefore, in addition to the project wells, six more wells were identified that had bulk density logs starting near the surface. The wells consisted of two from Merrill, two from Rudder, one from Benning, one from Darby, and none from Rogers as shown in the project layout in **Figure 3.1**.

Across the basin, the mineral compositions of the formations at shallower depths are considerably different than those at the depths of concern in the study. Most of the logs in the study begin around 5,000ft and substantial layers of low density halite (density=2.04 g/cm^3) and high density anhydrite (density=2.98 g/cm^3) exist in the first few thousand feet across much of the basin.

Significant washouts were apparent and common in all the shallow density logs and corrections had to be applied before calculations could be performed with the logs. These corrections were applied only to the specific logs used to calculate the shallow bulk density and not the broader project well set. A density of 2.55 g/cm^3 was assigned to any null values on the shallow bulk density log. This value was chosen because it balances the density values of anhydrite, halite, sandstone and shale. Next, the caliper readings were corrected for sudden jumps caused by the tool moving through a rugose hole. This was done by calculating the running average of the caliper over 4.5ft. The average was subtracted from the actual caliper reading. If the caliper deviated by more than 7/8in. from the running average then the density value at that point was assigned 2.55 g/cm^3. Then, the derivative of the caliper vs depth was calculated. A high derivative indicates that the caliper is pivoting too much in the hole to give accurate readings. If the derivative was greater than 0.5 or less than -0.5 then the density log was assigned a value of 2.55 g/cm^3 at that point. Next, logs were corrected for too low and too high density readings, possibly caused by the unfavorable hole conditions or mud cake buildup. It was assumed that 2.04 g/cm^3 should be the lowest density reading in the log. If any values were below this, then they were adjusted back to 2.04 g/cm^3. It was also assumed that 2.98 g/cm^3 should be the

highest density encountered in the well. If the density log had values above 2.98 g/cm^3, they were corrected back to 2.98 g/cm^3. Finally, if the caliper registered values above the maximum which the tool could reliably read, which was 16in. for each shallow density curve, then the density at those points was adjusted back to 2.55 g/cm^3. The final bulk density curves and overburden pressure curves with the preceding curves used to generate them are shown for three wells: Runk, Steele and Thayer in **Figure 3.11**.

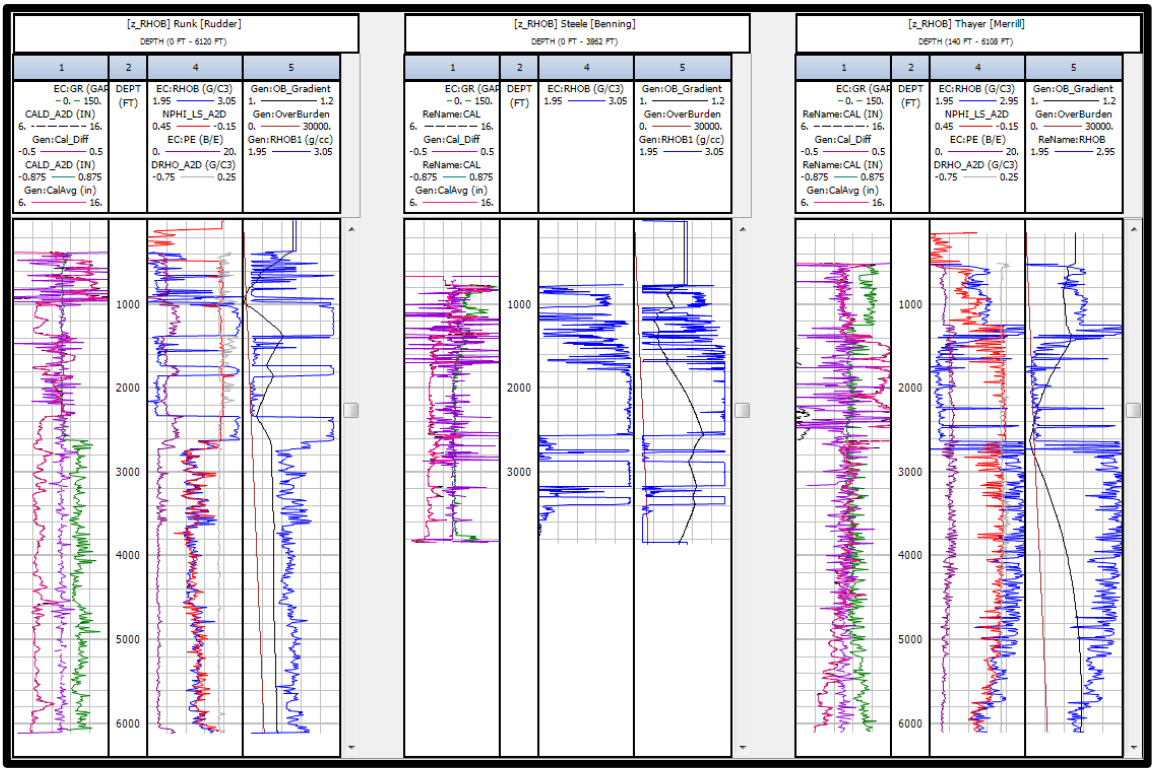

Figure 3.11. Sample shallow bulk density logs with applied corrections

The shallow overburden pressure was then calculated using the corrected shallow density logs. The shallow overburden was calculated by integrating the density curve

through the depth of the well. A density of 2.55 g/cm^3 was assumed for depths above the start of the curve and for any remaining null values. The curves were sampled at 0.5 foot intervals. The numerical integration equation used to calculate overburden pressure is shown below. TopDepth represents the depth at which the density curve starts in feet. All density readings are in g/cm^3.

$$Overburden_n = 2.55 \times TopDepth \times 0.433 + \sum_{i=TopDepth}^{n} (D_{i+1} - D_i) \times \frac{\rho_i + \rho_{i+1}}{2} \times 0.433 \quad (3.2)$$

Linear regression lines were fit to each shallow overburden pressure result in order to model the overburden pressure as a function of depth from 0-4,000ft, 0-5000ft, and 0-6,000ft. This allows for a more accurate shallow overburden pressure value which is based on the start of the project well's bulk density curve. The bulk density curves start between 4,000 to 6,000ft for most project wells. For example, if the well under investigation had a bulk density curve starting at 4,500ft, then the well's respective sub-area's regression line for shallow overburden of 0-5,000ft was used. The calculated regression equation table is shown in **Table 3.2.**

Well Name	Use for NCT well with ρ_b log starting: 0-3,000'	Use for NCT well with ρ_b log starting: 3,000'-4,000'
	Overburden Eqn of Line 0-3k'	Overburden Eqn of Line 0-4,000'
Thayer	-68.4300427 + 0.997919412 * DEPTH	-3.31681843 + 0.950865727 * DEPTH
Chaffin	-40.5652734 + 0.981614539 * DEPTH	-39.7059825 + 0.983189233 * DEPTH
Del	27.9997397 + 0.842070668 * DEPTH	-0.765347282 + 0.861289567 * DEPTH
Runk	2.43069354 + 0.950251726 * DEPTH	14.5125673 + 0.940257838 * DEPTH
Daren	15.420542 + 0.829153812 * DEPTH	
Steele	-41.8948862 + 1.12953068 * DEPTH	-36.898744 + 1.12626472 * DEPTH
Well Name	Use for NCT well with ρ_b log starting: 4,000'-5,000'	Use for NCT well with ρ_b log starting: 5,000'+
	Overburden Eqn of Line 0-5,000'	Overburden Eqn of Line 0-6,000'
Thayer	66.7065229 + 0.90991364 * DEPTH	106.919993 + 0.890341886 * DEPTH
Chaffin	30.6051779 + 0.942099784 * DEPTH	93.0250145 + 0.911726755 * DEPTH
Del	-28.8471495 + 0.87672842 * DEPTH	-39.8233049 + 0.881666756 * DEPTH
Runk	19.2389699 + 0.93721206 * DEPTH	25.6911185 + 0.933890925 * DEPTH
Daren		
Steele		

Table 3.2. Shallow overburden pressure regression equations

There were no shallow density logs in the Rogers sub-area. Therefore, the shallow overburden pressure is estimated by averaging the regression equation results for the nearest Rudder well (Daren) and the nearest Benning well (Steele). Well Daren's bulk density curve terminates at 2,475 ft. and well Steele's at 3,843ft. So there is only one regression equation for both these wells. Their regression equations are built from 0-2,475ft and 0-3,843ft, respectively. The Merrill sub-area has two wells with shallow bulk density curves. For project wells in the Merrill sub-area, the average of the two shallow density regression equations was used. Project wells in sub-areas with only one shallow density well were assigned the overburden pressure regression equation from their sub-area's one shallow density well.

3.8 Applying Eaton's Equation for Pore Pressure Estimation

With the shallow overburden pressure modeled, the total overburden pressure for all the wells under investigation was then calculated. The shallow overburden pressure calculated for each investigated well was converted to an apparent bulk density. This was done so that the investigated well's density log would extend from the actual start of the bulk density curve to the surface. The conversion to apparent density was calculated with:

$$\rho_{app} = \frac{P_{OB_{shallow}}}{0.433 \times TopDepth} \tag{3.3}$$

The overburden pressure was then calculated by integrating the density curve using the same numerical integration method employed for the shallow density. Any null values were assigned the calculated apparent density value.

Hydrostatic pressure was then calculated through the depth of each well. Recall that the hydrostatic pressure is important because it is the same as the normal pore pressure. Overlaying the hydrostatic pressure on the calculated pore pressure allows for the rapid identification of overpressure and the magnitude above normal pressure at each depth. The hydrostatic pressure is calculated with:

$$P_{Hydro} = 0.433 \times \rho_w \times D \tag{3.4}$$

where ρ_w is the density of formation water in g/cm^3 and depth, D, in feet. Due to variability of formation water salinity and lack of reliable data, formation water density was assumed

to be 1.03 g/cm^3 for the entirety of the logging interval. This density corresponds to a 65kppm brine at 140°F.

Eaton's **Equation 1.8** was then employed to calculate pressure at each depth. Here, for each depth on the log, P_{OB} is the calculated overburden pressure in psi. P_{Hydro} is the hydrostatic pressure in psi. ΔT_{ob} is the observed value from the sonic log. ΔT_{norm} is the normal ΔT reading from the sonic log, which is the value of the NCT line at the corresponding depth.

Finally, the deviation between the calculated pore pressure and normal pore pressure was calculated. A positive ΔP represents overpressure, as shown below.

$$\Delta P = P - P_{Hydro} \tag{3.5}$$

This process was performed twice for each well. First for the shale and second for the sand trend. The only variable to change between the sand and shale trend is ΔT_{norm} as used in Eaton's **Equation 1.8.** An example output plots with NCTs and pressure curves is shown in **Figure 3.12**.

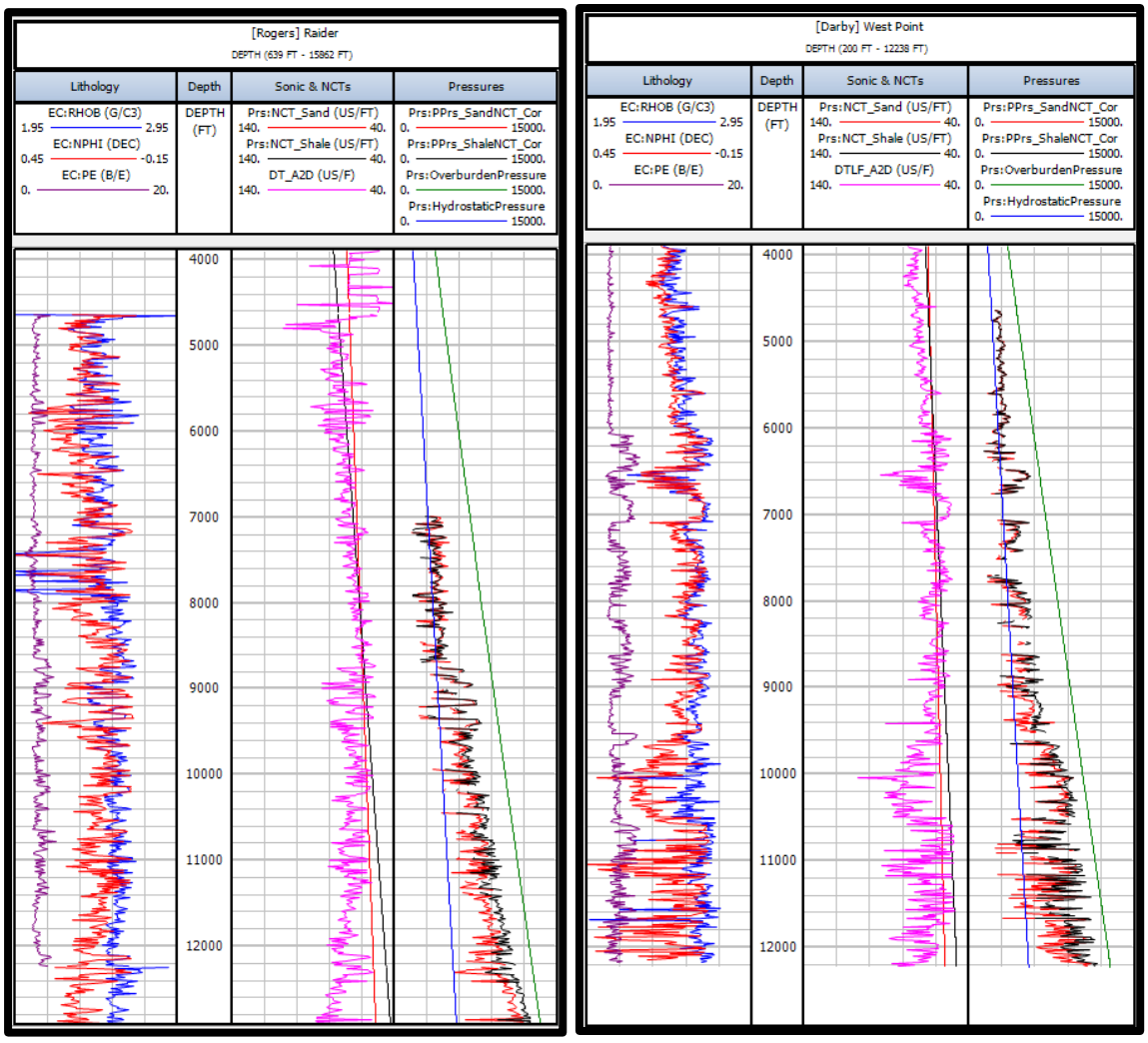

Figure 3.12. Pressure curves for wells Panjwai and Lewis

The first track, Lithology, shows the environmetally corrected bulk density, neutron porosity, and photoelectric factor. The third track shows the sand NCT in red, the shale NCT in black, and the sonic curve in pink. The fourth track, Pressures, shows the calculated pore pressure from the sand NCT in red, the calculated pore pressure from the shale NCT in black, the overburden pressure in green, and the hydrostatic pressure in blue.

3.9 Validating Pressure Estimates

After pressures were calculated from the sand and shale trend lines using Eaton's equation, the pressure estimates were validated against actual pressure data from a drill stem test, flow back following completion operations, and managed pressure drilling data.

3.9.1 Drill Stem Test

A DST was the first method employed to validate the pressure estimations from the model. The DST was conducted in the Benning sub-area, the same sub-area as wells Airborne and Sperwan, as shown in **Figure 3.1**. For the DST, the well was flowing for 24 hours and then shut in for 116 hours and 20 minutes. The formation pressure at mid perforation, 10,562ft, was determined to be 8,013psi. There were no nearby producing wells at the time of the test.

Sperwan and Airborne's corresponding formation zone to the DST well was found using gamma ray logs. Sperwan's corresponding depth was found to be 11,176ft and Airborne's corresponding depth was 11,383ft. The gamma ray curve and pressure calculations for each well are displayed in **Figure 3.13**. A conservative normal pressure gradient of 0.465 psi/ft was assumed in order to correct for the depth difference between the DST validation well and the two project wells as summarized in **Table 3.3**.

DST TVD [ft]	DST Pressure [psi]	Equivalent Pressure at Target Depth of 11,383ft (Airborne) [psi]	Equivalent Pressure at Target Depth of 11,176ft (Sperwan) [psi]
10,562	8,084	8,466	8,370

Table 3.3. Drill stem test validation well and equivalent pressures

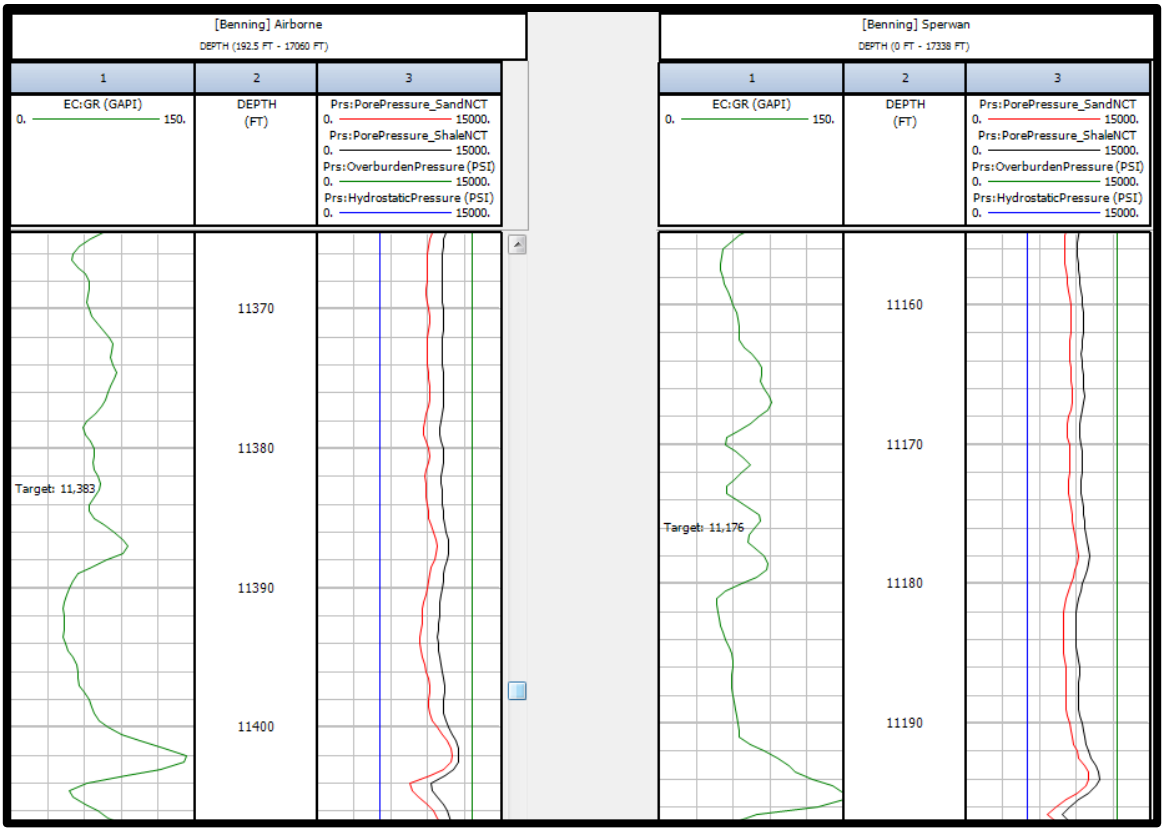

Figure 3.13. Estimated pressures and gamma ray logs for wells Airborne (left) and Sperwan (right)

The green curve is the environmentally corrected gamma ray log (EC:GR), the red curve is the estimated shale pore pressure (Gen:Pore- Pressure), and the black curve is the estimated sand pore pressure (Gen:PorePressure_Sand).

The DST measured the formation pressure in the 3rd Bone Spring Sand. This is mixed lithology layer overlaying the Wolfcamp formation. The 3rd Bone Spring Sand is comprised primarily of dolomitic sands interbedded with thin shale layers. This is illustrated with the mineral overlay of the apparent matrix density vs apparent volumetric photoelectric factor cross plot of the 3rd Bone Spring Sand for well Sperwan after removing data points containing TOC, as shown in **Figure 3.14**. But, given the ΔT difference between sand and dolomite (56μs/ft vs 44μs/ft, respectively) it would be

expected that the dolomite trend would approach closer to vertical than the sand or shale trend. It follows then that for a dolomitic sand as in the 3rd Bone Spring Sand, a sand trend line would tend to over predict the pressures.

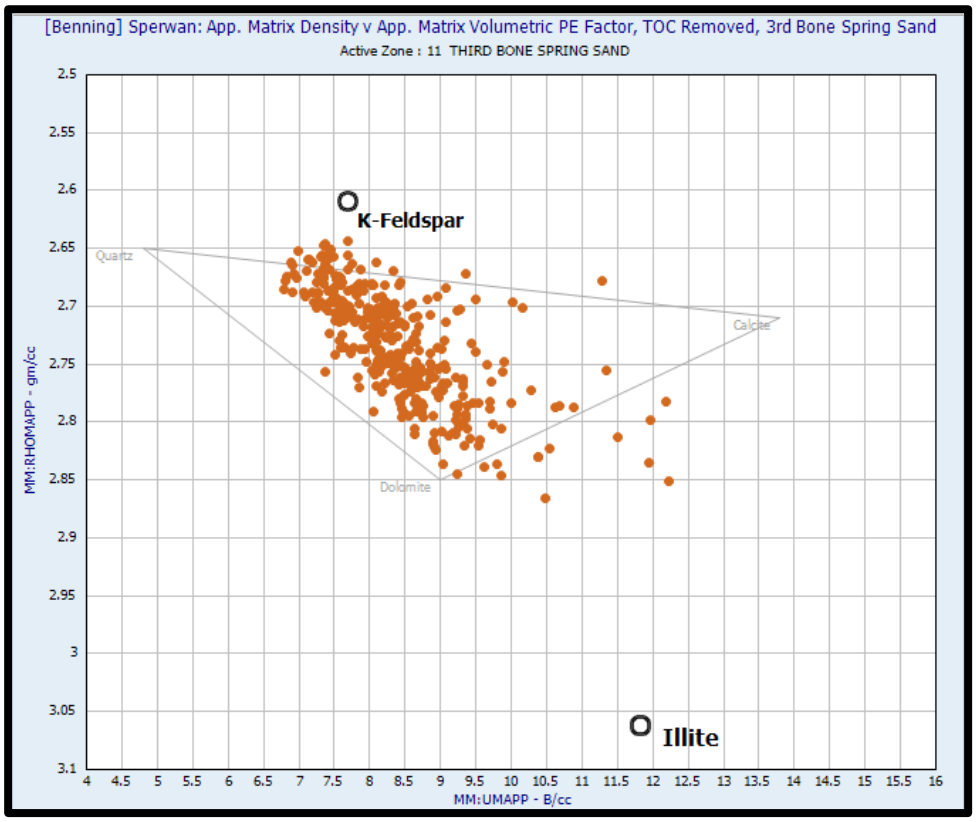

Figure 3.14. Apparent matrix density vs. apparent matrix volumetric photoelectric factor, well Sperwan, Third Bone Spring Sand, data points containing TOC removed

The pressure from the sand and shale trend at the equivalent depths in both Sperwan and Airborne were measured. Additionally, an average pressure across a 5ft interval centered on the equivalent depth was measured to account for spacing within the drill stem test packers. **Figures 3.15** and **Figure 3.16** both highlight the narrow scope of

investigation for the pressure calculations. For the sand and shale trend pressure calculations for Sperwan and Airborne, the calculated pressure was higher than the equivalent DST pressure. As outlined earlier, this is expected for measuring dolomitic sands with a sand trend line.

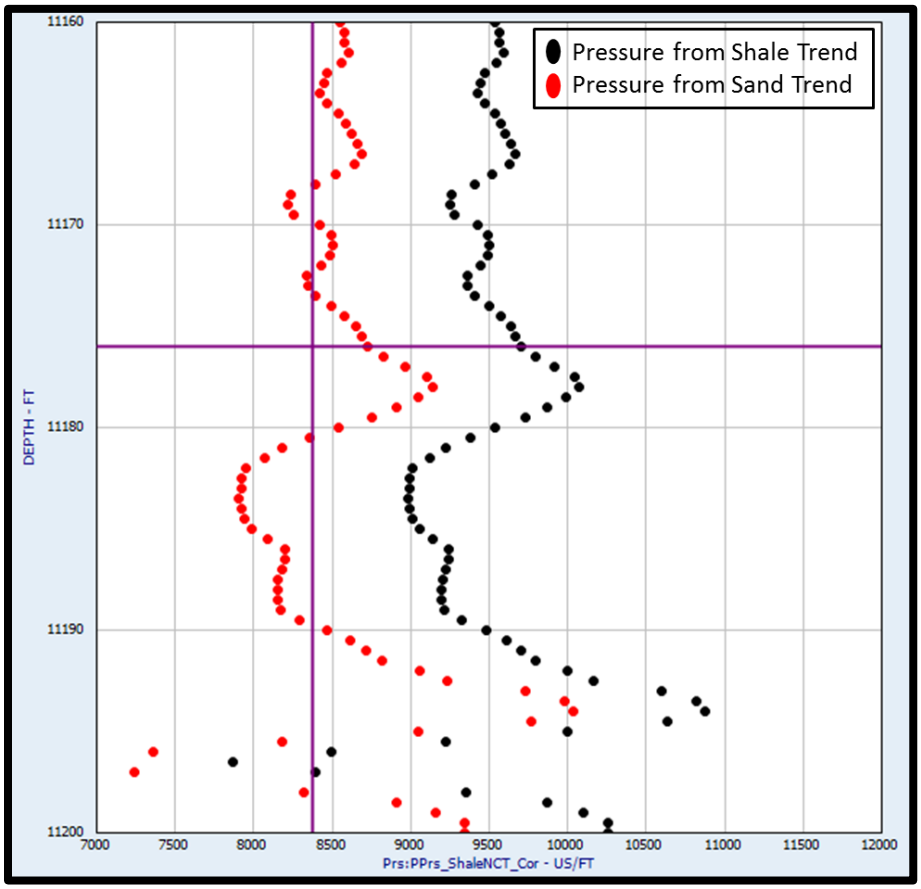

Figure 3.15. Enhanced picture of Sperwan's depth vs estimated pressure

The horizontal purple line represents the equivalent depth in Sperwan to the DST depth, based on gamma ray readings. The horizontal purple line represents the equivalent pressure in the Sperwan well based on a 0.465 psi/ft pressure gradient.

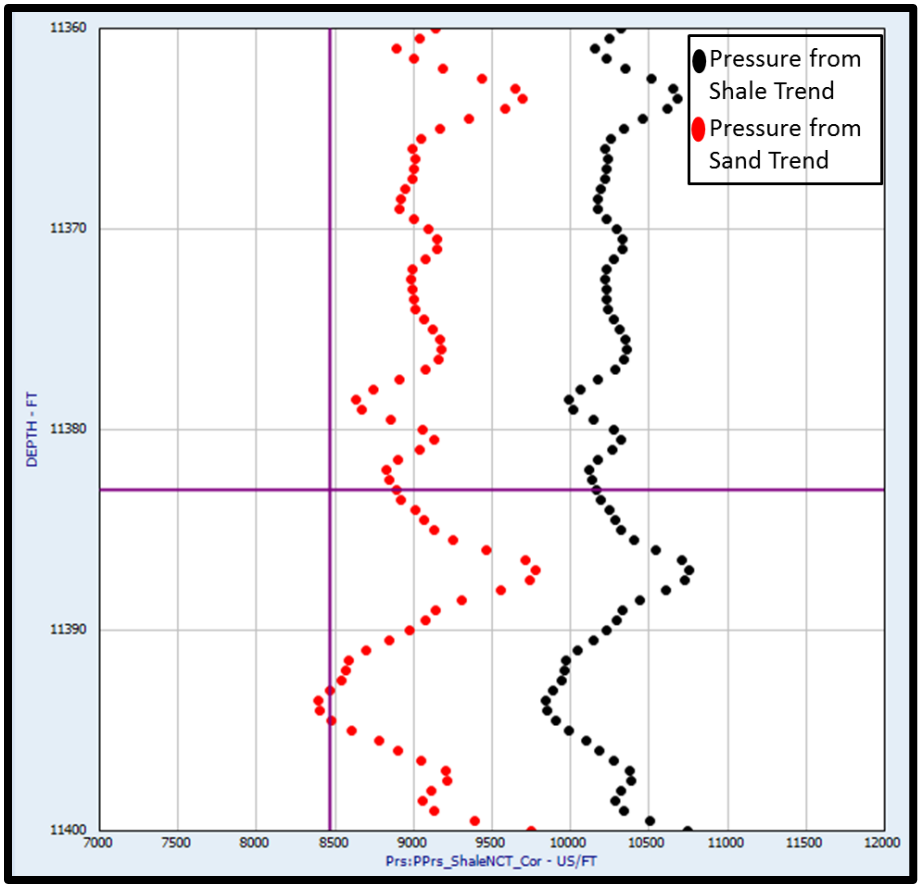

Figure 3.16. Enhanced picture of Airborne's depth vs estimated pressure
The vertical purple line represents the equivalent depth in Airborne to the DST depth, based on gamma ray readings. The horizontal purple line represents the equivalent pressure in the Airborne well based on a 0.465 psi/ft pressure gradient.

Examining the results in **Table 3.4**, we see that the shale and the sand both overestimate the pressures for the 3rd Bone Spring Sand. The gap can be attributed partially to the fact that the DST was preformed over 15 miles south of the project wells and that the formation is neither a clean sand nor clean shale. Insight can be gleaned from the data though with regards to how well coupled the 3rd Bone Spring Sand is in vicinity of Sperwan and Airborne. Sperwan shows a 971 psi difference between the shale and

sand readings while Airborne shows a 1,238 psi difference, based on pressure at the target depth. The same general trend holds for the 5ft. interval as well. The higher difference between the sand and shale pressure could be taken to indicate a lesser coupled formation.

Well	Pressure Trend	Target Depth [ft]	Pressure at Target Depth [psi]	Target Depth Pressure Minus DST Equivalent Pressure [psi]	Avg. Pressure at Target Depth +/- 2.5 ft [psi]	Avg. Pressure Minus DST Equivalent Pressure [psi]	% Difference of Average Pressure
Sperwan	Shale	11,176	9,704	1,334	9,755	1,385	17%
Sperwan	Sand	11,176	8,726	356	8,784	414	5%
Airborne	Shale	11,383	10,164	1,698	10,238	1,772	21%
Airborne	Sand	11,383	8,887	421	9,000	534	6%

Table 3.4. Estimated pressure comparison between Sperwan, Airborne and the DST validation well

3.9.2 Flowback

To further validate the model, the reservoir pressures from four wells in the Rudder sub-area were calculated from flowback back data following a frac job. The calculated reservoir pressures for each well are shown in **Table 3.5**. The wells are laid out as shown previously in **Figure 3.1**. The horizontal wells were completed in one of the sandy pay zones in the upper Wolfcamp or the 2nd Bone Spring Sand. Since the flowback data follows a fracture treatment, it was assumed that the pressure in the validation wells is a representation of the average pressure spanning from the top of the Wolfcamp to the bottom of the lower sandy pay zone common across the Rudder sub-area. The corresponding target intervals in each of the three Rudder sub-area wells were identified using gamma ray curve readings. The sand NCT was found for each of the three Rudder wells using the same methods as previously outlined. The pressures were corrected to

account for differences in depth between the validation wells and the interval midpoint for the Rudder wells. The pressure was corrected for depth differences at +/- 0.465 psi/ft.

Well	Formation	TVD [ft]	P_{Csg} @ HC Show [psi]	Calc P_{wf} [psi]
Validation Well 1	2nd BS Sand	8,360	810	4,553
Validation Well 2	Upper Wolfcamp Sand	9,655	2,500	6,821
Validation Well 3	Upper Wolfcamp Sand	9,273	1,690	5,840
Validation Well 4	Upper Wolfcamp Sand	9,575	2,600	6,885

Table 3.5. Rudder area estimated pressure from flowback data

P_{csg} @ HC Show in column 4 is the recorded casing pressure at the surface when the first hydrocarbon appeared in appreciable quantities. The "Calc P_{wf}" is the calculated reservoir pressure as calculated with ***Equation 1.6.***

Validation Well 3 lies approximately ten miles northwest from the general center of the other validation wells. Validation Wells 2, 3, and 4 were completed in the same pay zone. The calculated pressures from the sand trend for each project well were higher than the formation pressure estimated from flowback data in Validation Well 3, as noted in **Table 3.5**. Well Buckner is in close agreement with Validation Well 3 but differs by almost 10% from Validation Wells 2 and 4. The opposite is true for wells Kandahar and Masum Ghar. Bucker is the closest project well to Validation Well 3. This may be an indication of a structural change or lithology change that occurs between Buckner and Validation Well 4. The 2nd Bone Spring Sand well, Validation Well 1 presents discrepancies as discussed in the DST measurement section. In each case with Validation Well 1, the estimated pressures with the project wells were higher than the flowback estimated pressures.

Project Well	Formation	Comparison Well	Zone Top [ft]	Zone Bottom [ft]	Zone Center [ft]	Mean Sand Pore Pressure [psi]	Depth Difference between Project Well and Validation Well [ft]	Equivalent Pressure Difference from Depth Difference [psi]	Equivalent Validation Well P_{wf} [psi]	Project Well Mean Sand Pore Pressure minus Equivalent Validation Well P_{wf} [psi]	% Difference
Kandahar	2nd BS Sand	Validation Well 1	7,408	7,698	7,553	5,129	-807	-375	4,178	951	22.8%
Kandahar	Upper Wolfcamp Sand	Validation Well 2	9,137	9,223	9,180	6,530	-475	-221	6,600	-70	-1.1%
Kandahar	Upper Wolfcamp Sand	Validation Well 3	9,137	9,223	9,180	6,530	-93	-43	5,797	733	12.6%
Kandahar	Upper Wolfcamp Sand	Validation Well 4	9,137	9,223	9,180	6,530	-395	-184	6,701	-171	-2.6%
Buckner	2nd BS Sand	Validation Well 1	7,530	7,712	7,621	4,696	-739	-344	4,210	486	11.6%
Buckner	Upper Wolfcamp Sand	Validation Well 2	9,235	9,340	9,288	6,008	-368	-171	6,650	-642	-9.7%
Buckner	Upper Wolfcamp Sand	Validation Well 3	9,235	9,340	9,288	6,008	15	7	5,847	161	2.8%
Buckner	Upper Wolfcamp Sand	Validation Well 4	9,235	9,340	9,288	6,008	-288	-134	6,751	-743	-11.0%
Masum Ghar	2nd BS Sand	Validation Well 1	8,144	8,421	8,283	5,609	-78	-36	4,517	1,092	24.2%
Masum Ghar	Upper Wolfcamp Sand	Validation Well 2	9,601	9,695	9,648	6,725	-7	-3	6,818	-93	-1.4%
Masum Ghar	Upper Wolfcamp Sand	Validation Well 3	9,601	9,695	9,648	6,725	375	174	6,015	710	11.8%
Masum Ghar	Upper Wolfcamp Sand	Validation Well 4	9,601	9,695	9,648	6,725	73	34	6,919	-194	-2.8%

Table 3.6. Rudder area project wells compared to flow back validation wells

In **Table 3.6**, "Zone Top" and "Zone Bottom" in columns 3 and 4 represent the height of the interval across which the pressure is averaged. The "Mean Sand Pore Pressure" is the average pressure across the zone as calculated from the sand NCT. The "Depth Difference" is the difference in the depth of the center of the zone of the project well from the validation well. The "Equivalent Pressure Difference" is the "Depth Difference" multiplied by 0.465 psi/ft. The "Equivalent Actual Well P_{wf}" is the equivalent validation well formation pressure after it has been corrected for differences in depth by adding the validation well "Calculated P_{wf}" from **Table 3.5** to "Equivalent Pressure Difference". With these calculations, P_{wf} is assumed to be representative of initial reservoir pressure.

3.9.3 Managed Pressure Drilling

The daily drilling records for four wells in the Benning sub-area which were drilled using MPD were examined to extract information to estimate the reservoir pressure. Mud is circulated through the chokes during MPD and the casing pressure while making drill pipe connections, mud weight, and atmospheric pressure are used to calculate reservoir pressure as outlined in **Equation 1.5**. It is assumed that the pressure communicating with the wellbore is coming from the pay zone drilled in the lateral. This assumption was verified with geosteering data available for each well. These pay zones are between 10-20ft thick. The calculated reservoir pressures for the validation wells are shown in **Table 3.7**. **Figure 3.1** portrays the spatial distribution of the project and validation wells across the Benning sub-area. The pressures in the project wells are calculated from a generated sand NCT. The calculated pressure estimates across the corresponding pay zone is then

corrected for the depth differences between project wells and the validation wells at +/- 0.465 psi/ft.

Validation Wells X, Y, and Z had no nearby adjacent wells producing from the same formation. Validation Well W had multiple adjacent wells producing from the same formation. Therefore, it was expected that the model would estimate a higher pressure than what was calculated with MPD data in Validation Well W. The general log suite and resultant pressures curves in the zone of interest for Well Sperwan are shown in **Figure 3.17**. As with the previous wells, the shale NCT leads to a higher calculated pressure than the sand trend for Sperwan, as seen in track 6 of **Figure 3.17**, with the pressure from the shale trend as the black curve the pressure from the sand trend as the red curve.

Well	Formation	Calculated P_{wf}
Validation Well W	Wolfcamp Upper Sand A	7,746
Validation Well X	Wolfcamp Upper Sand A	8,329
Validation Well Y	Wolfcamp Upper Sand B	9,350
Validation Well Z	Wolfcamp Upper Sand A	8,272

Table 3.7. Benning area reservoir pressures from managed pressure drilling data

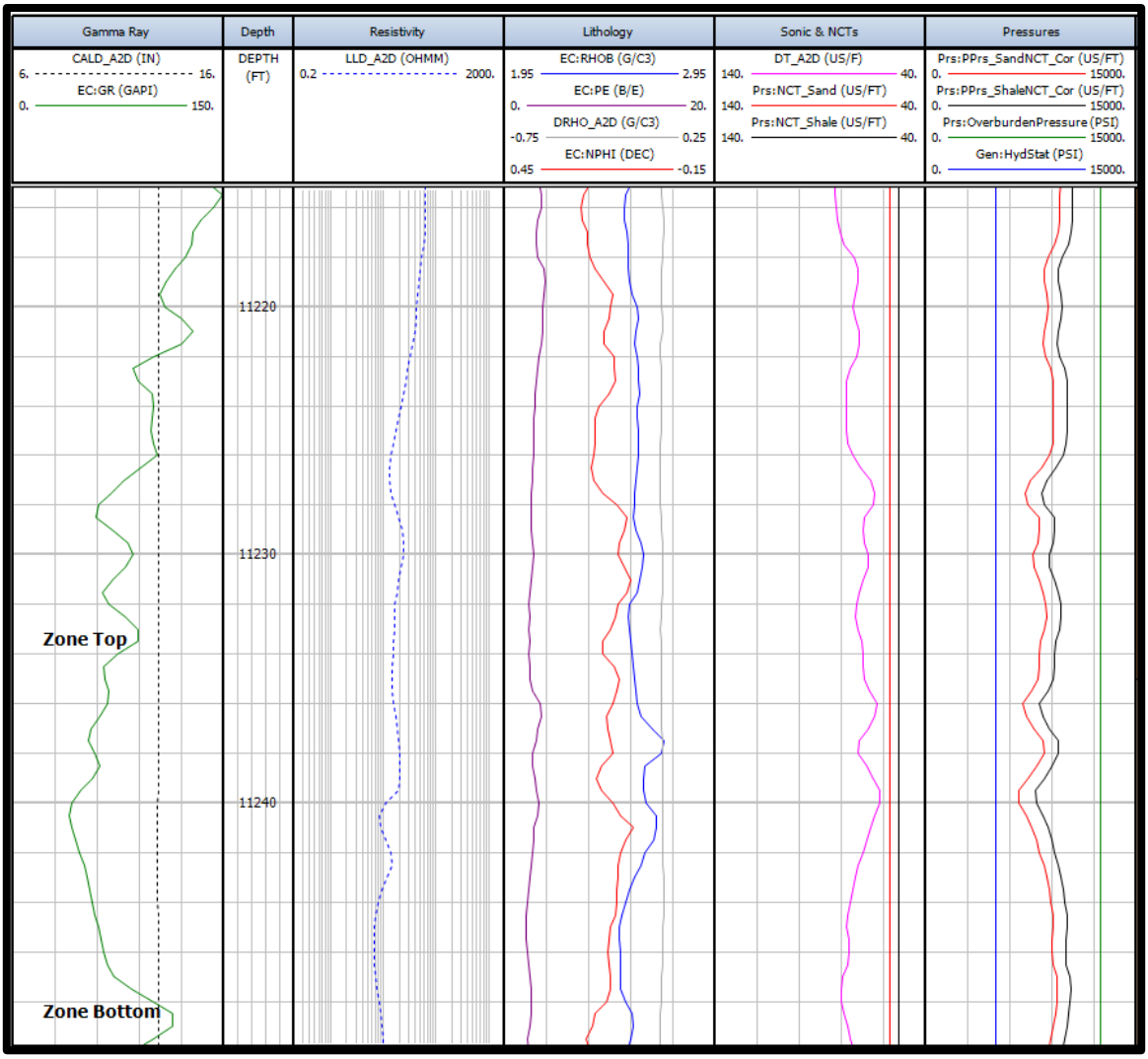

Figure 3.17. Sperwan well's log readings in Upper Wolfcamp pay zone

Expanding out the calculated pore pressure from the sand NCT highlights the importance of precision in the measurements, as demonstrated in **Figure 3.18**. A macro view of the calculated pore pressure from the sand trend line for the Sperwan well suggests an over estimation of formation pressure. But, as the Wolfcamp Upper Sand A pay zone

interval is zoomed in on, the pressure estimation becomes much more reasonable. Additionally, some error is to be expected in the measurements as production history in the basin shows fluctuations in initial pressures within the same pay interval in the same area. Pressure estimation accuracy will continue to improve as more wells are added to future studies to cover a greater area.

As shown in **Table 3.8**, both Sperwan and Airborne overestimate the pressures in Validation Well W, which is expected given its adjacent well production history. Sperwan falls within <|1%| in the remaining two well's with Wolfcamp Upper Sand A formation pressure estimations. Airborne overestimates the pressure in the Validation Well X and Validation Well Z by an average of 8.25%. Though, Airborne is a near perfect match to the Wolfcamp Upper Sand B for Validation Well Y with only a 2 psi difference. Sperwan underestimates the pressure in Wolfcamp Upper Sand B of Validation Well Y by 8.2%.

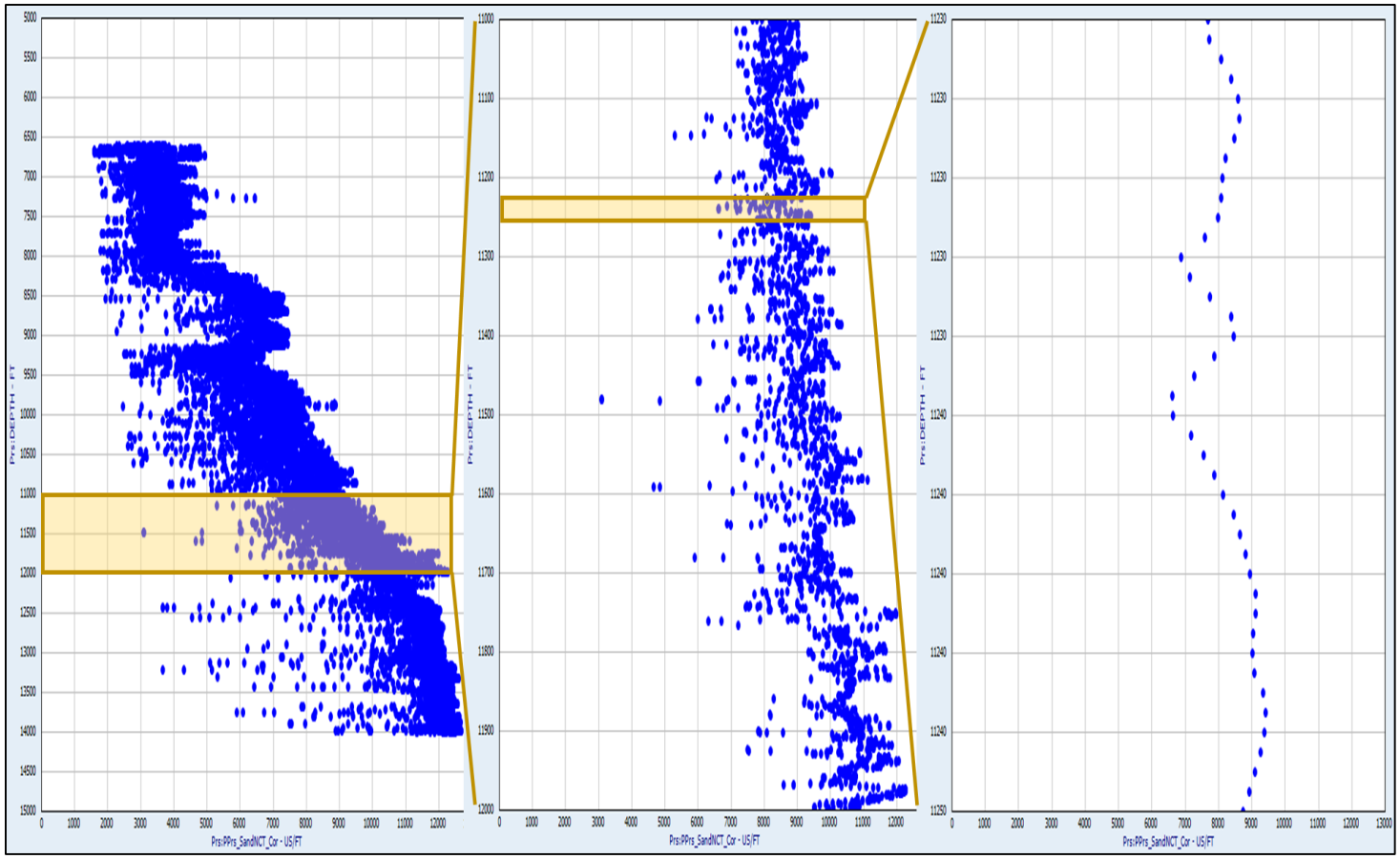

Figure 3.18. Expansion of depth vs the calculated pore pressure from the sand trend line

Validation Well	Well	Formation	Top [ft]	Bottom [ft]	Avg Depth [ft]	Avg. Pressure from Model [psi]	Δ Depth b/t Wells [ft]	Pressure Correction (0.465* Δdepth) [psi]	Validation Well P_{wf} + Pressure Correction [psi]	Difference b/t depth corrected pressure and model pressure [psi]	Percent difference of validation well's P_{wf} [psi]
Validation Well W	Sperwan	Wolfcamp Upper Sand A	11234	11248	11241	8349	501	233.0	7,978.67	370	4.8%
	Airborne	Wolfcamp Upper Sand A	11443	11453	11448	9204	708	329.2	8,074.92	1,129	14.6%
Validation Well X	Sperwan	Wolfcamp Upper Sand A	11234	11248	11241	8349	51	23.7	8,352.92	(4)	-0.04%
	Airborne	Wolfcamp Upper Sand A	11443	11453	11448	9204	258	120.0	8,449.18	755	8.1%
Validation Well Y	Sperwan	Wolfcamp Upper Sand B	11340	11367	11354	8740	346.5	161.1	9,511.08	(771)	-8.2%
	Airborne	Wolfcamp Upper Sand B	11541	11563	11552	9605	545	253.4	9,603.38	2	0.0%
Validation Well Z	Sperwan	Wolfcamp Upper Sand A	11234	11248	11241	8349	301	140.0	8,412.10	(63)	-0.76%
	Airborne	Wolfcamp Upper Sand A	11443	11453	11448	9204	508	236.2	8,508.35	696	8.4%

Table 3.8. Wells Sperwan and Airborne's estimated pressures compared to MPD validation wells

The results are displayed graphically in **Figure 3.19**. All the validation wells in the Benning sub-area also had reservoir pressure estimates computed from flowback data. The horizontal lines on the graphs offer a comparison of the spread in estimates possible with both managed pressure drilling and flow back estimates. The estimated pressure from Airborne and Sperwan are plotted on the same level of each well to highlight the range in the estimates.

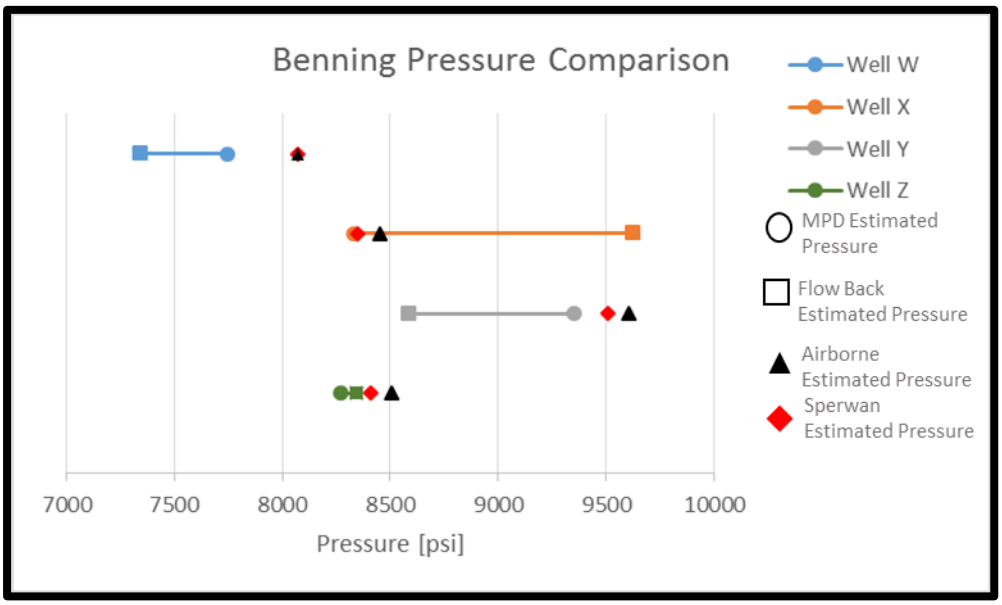

Figure 3.19. Pressure estimation spread in Benning sub-area for MPD, flowback, and well log estimates

4. DISCUSSION

Herein we are extending the usefulness of Eaton's equation and offering an explanation of the differences observed between the pressure estimates from sand and shale trends. Eaton's original methodology for estimating pore pressure from sonic logs was successfully expanded in this project to include the use of a sand lithology in the Delaware Basin. The new pressure prediction is validated in the Delaware Basin using DST data, flowback data, and managed pressure drilling data.

While the coupling of pressure from the kerogen bearing organic-rich mudstone layers to the conductive lamination may have a direct bearing on the production performance of wells, a detailed study of the production is beyond the scope of this study and is left to a future investigations. However, an indication of coupling can be derived, again using Eaton's equation on a different lithology. The initial pressure estimations drawn from the shale normal compaction trends are affected by the kerogen maturation process. The elevated pressure within the organic pore space in the kerogen resulting from hydrocarbon generation is not necessarily accounted for using Eaton's original formation pressure estimation method. Some of the generated hydrocarbons within the organic pores are not coupled to the conductive laminations do to permeability constraints. Thus, it should generally be expected that the pressures predicted with the shale NCT will be greater than what is measured with a formation pressure measurement method. This differential may be a direct indication of the coupling of a low permeability lithology to the conductive laminations.

To investigate the causes of the overpressure, the pore pressure as determined using Eaton's equation is utilized together with the vitrinite reflectance data. The overpressure magnitude and depths are then compared to the LOM through the depth of the well.

Looking at overpressure as the calculated pore pressure from Eaton's equation minus the hydrostatic pressure allows for the investigation of the pressure and kerogen maturity relationship. Plotting the magnitude of overpressure versus LOM reveals significant insight into the driver of overpressure in the basin as shown in **Figure 4.1**. The overpressure remains relatively low and constant for all wells across the basins until the kerogen reaches a LOM of 8. The LOM of 8 corresponds to a Ro of 0.56 which is where the kerogen begins moving into the peak oil generation window. At an LOM of 10, corresponding to a Ro of 0.8, the overpressure begins to increase rapidly in a nearly linear trend. This corresponds to the start of the wet gas generation and with oil generation near its maximum. At LOM 11.5 the overpressure slope begins to reduce, corresponding to the oil window floor. At LOM 13.5 another change in the overpressure slope is observed as it again reduces and corresponds to the end of the wet gas generation window. Data extending through the dry gas window shows a continued increase in overpressure as the kerogen produces dry gas.

These observations show that in the Delaware Basin, the hydrocarbon generation stage windows are tied to the rate of change in overpressure. The onset of hydrocarbon generation clearly corresponds to the rapid increase in overpressure. Overpressure increases at greater rates as wet and dry gas generation begins in addition to the continued oil generation. The rate of the overpressure increase slows as the kerogen enters the later

stages of maturation and produces predominately dry gas. These observations lead to the conclusion that hydrocarbon generation is drives overpressure in the Delaware Basin.

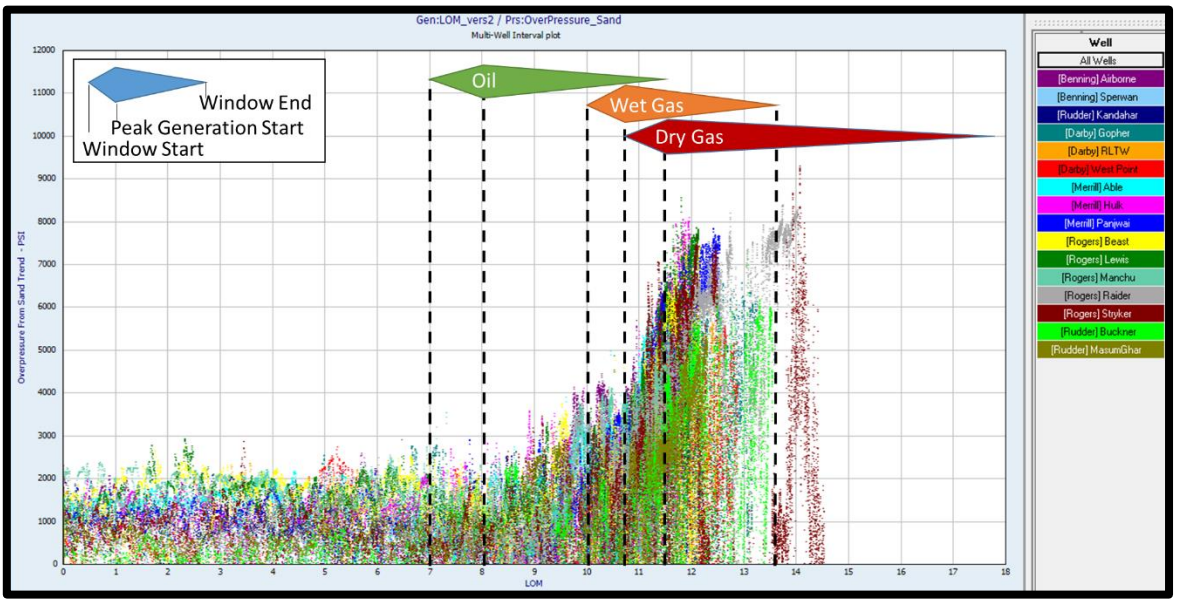

Figure 4.1. Overpressure vs LOM for all wells in study

On close examination, some of the wells tend the reach the slope changes slightly earlier or later than expected. The LOM curve in the study is a function of the Ro regression line which is based on limited data from the USGS study. But, now LOM can linked to overpressure. This may enable the prediction of kerogen maturity based on the shape and distribution of the well's overpressure curve as calculated from Eaton's equation. This becomes much more apparent as the wells are separated again by area and display similar responses as shown in **Figures 4.2a-e**.

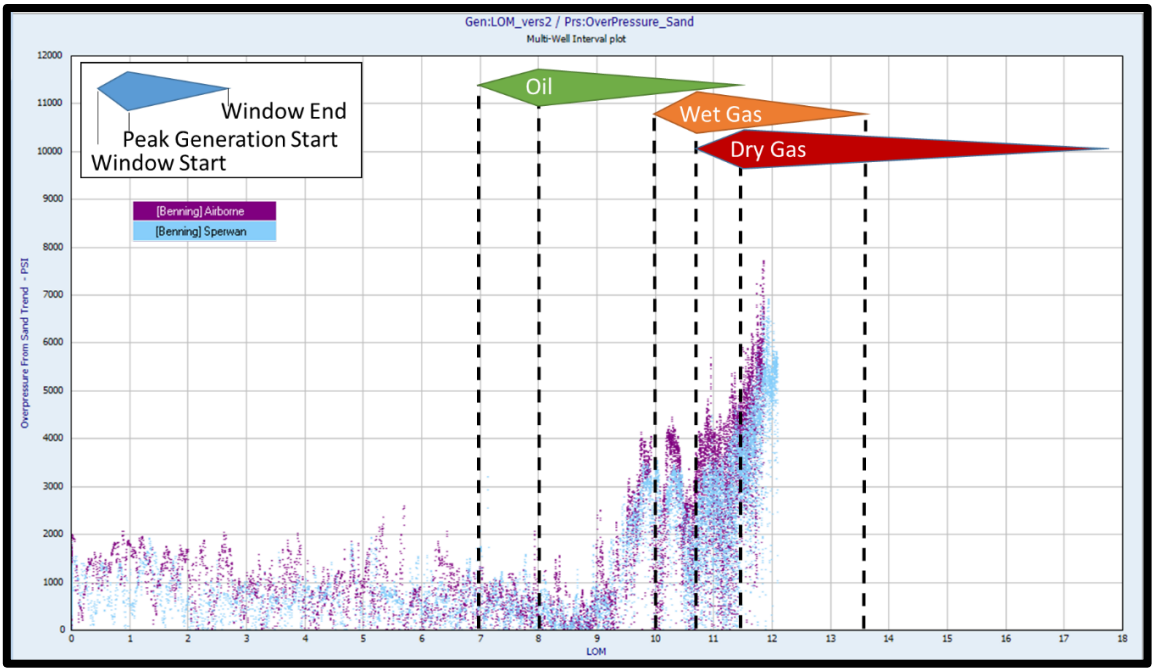

Figure 4.2a. Overpressure vs LOM for Benning area wells

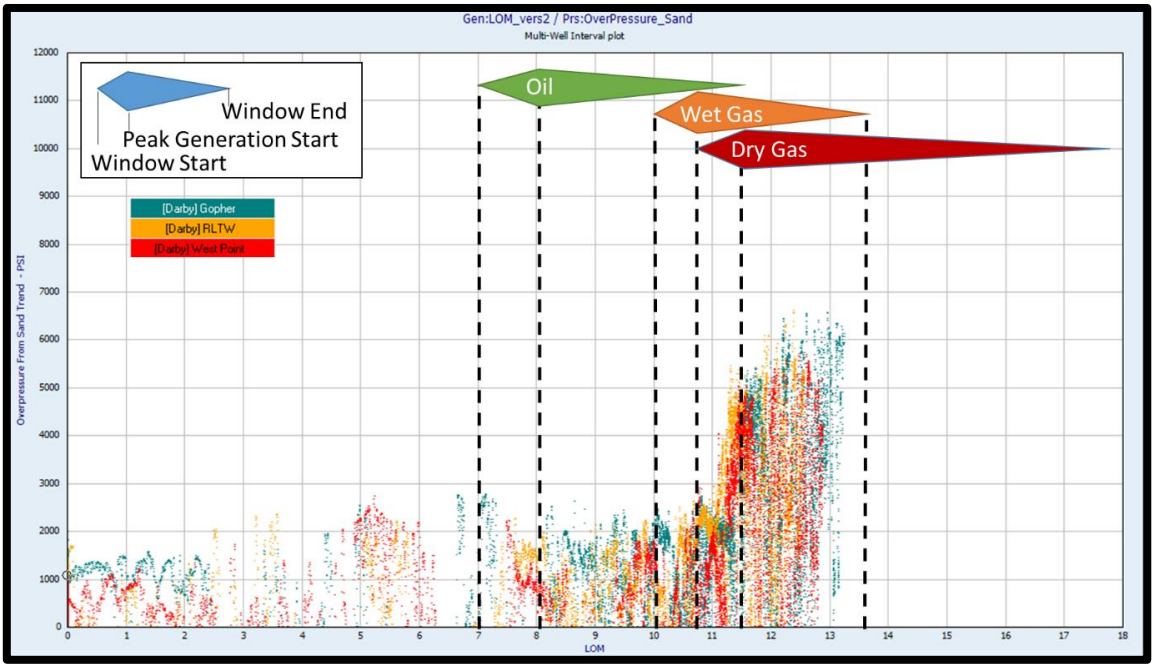

Figure 4.2b. Overpressure vs LOM for Darby area wells

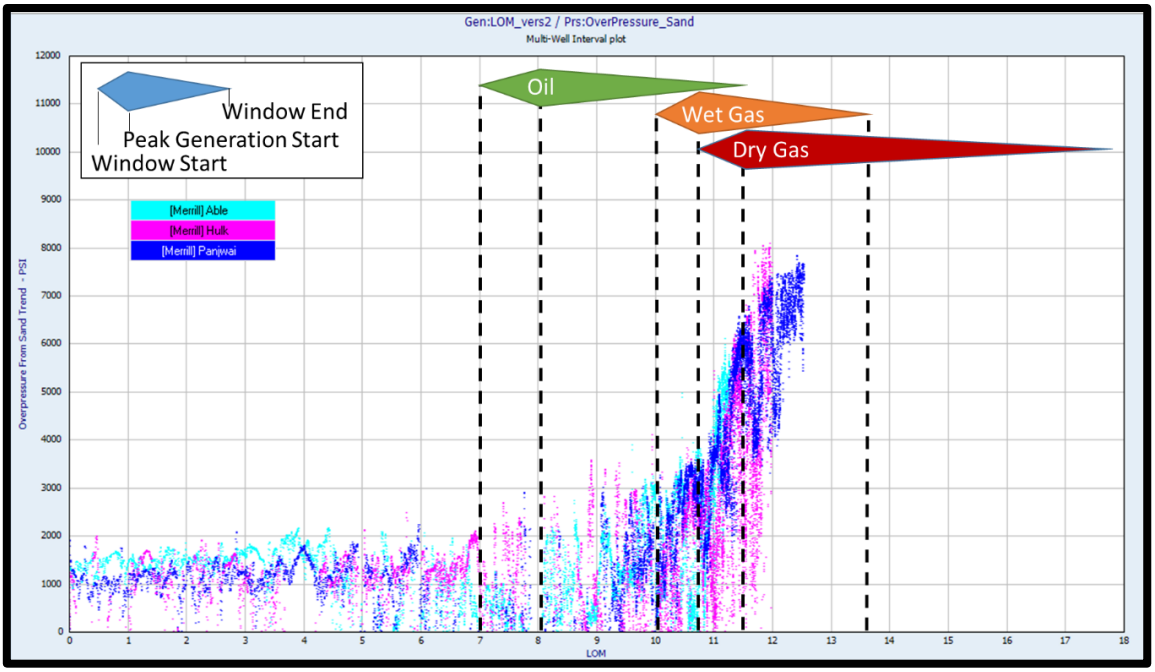

Figure 4.2c. Overpressure vs LOM for Merrill area wells

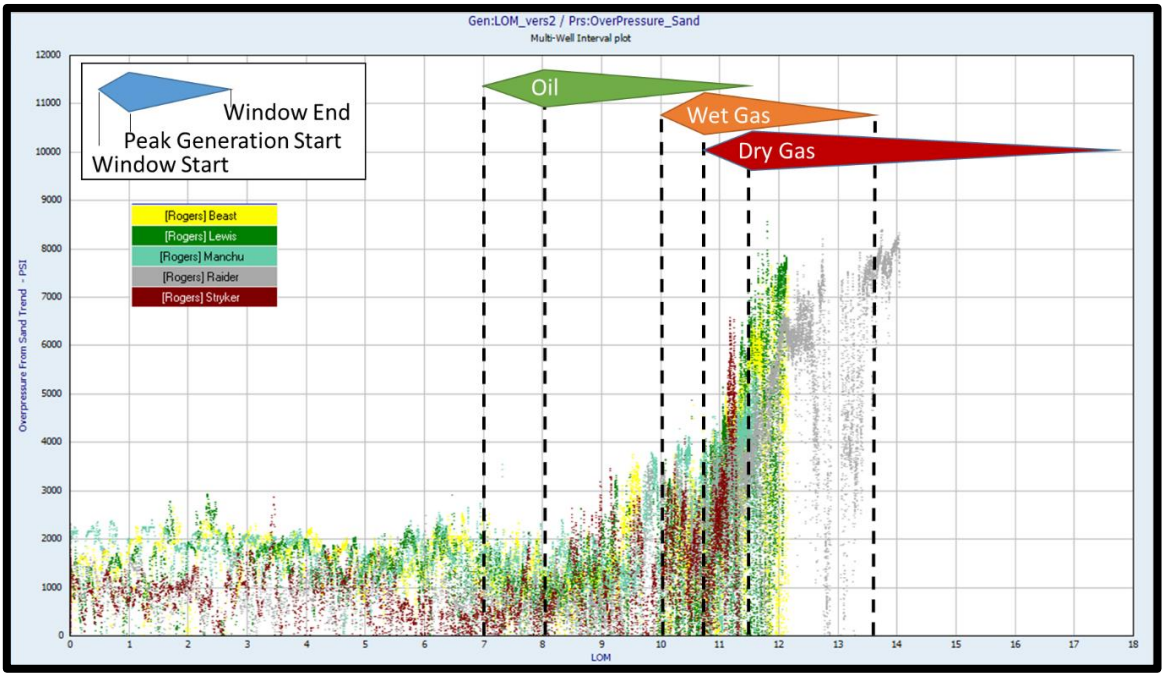

Figure 4.2d. Overpressure vs LOM for Rogers area wells

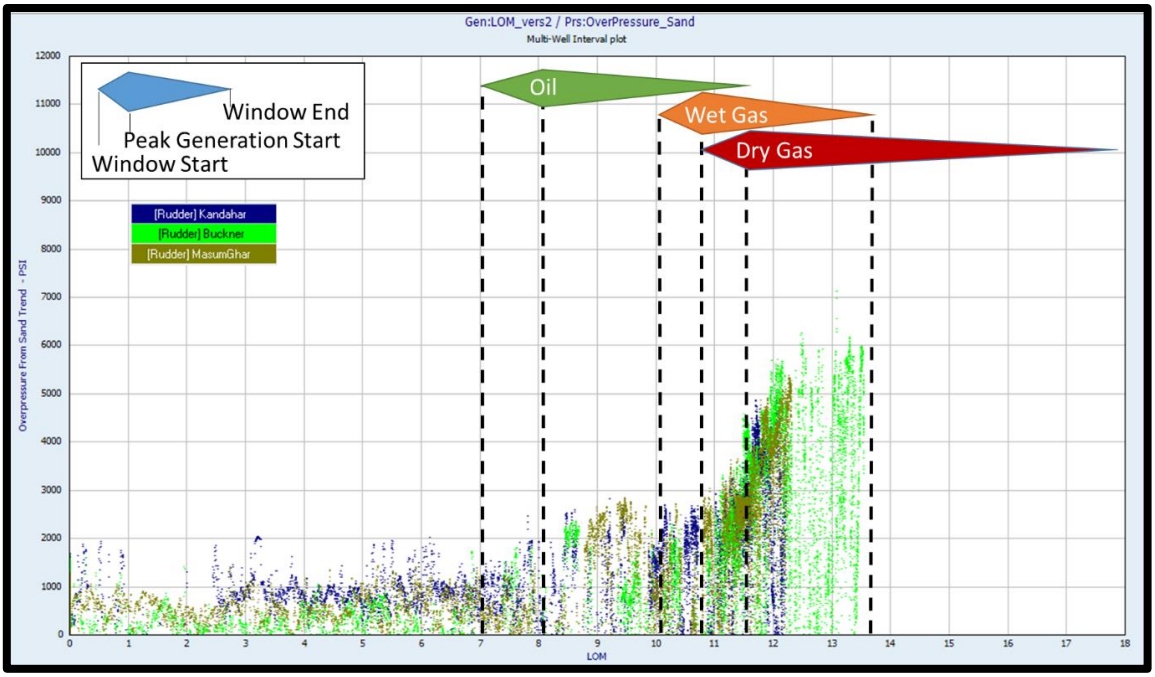

Figure 4.2e. Overpressure vs LOM for Rudder area wells

5. CONCLUSIONS

This study has produced important conclusions:

1. Eaton's method can be modified by using the sand NCT to predict the magnitude of overpressure using the sonic log in the Delaware Basin.
2. Kerogen maturity is the key driver of the overpressure in the Delaware Basin.
3. The magnitude of overpressure can offer insight into how well connected the organic pores are to the matrix.
4. The thermal maturity maps for the basin may possibly be refined based on the calculated overpressure vs LOM from sonic logs.

These conclusions are important in building an accurate petrophysical model of the basin which can serve to strengthen the strategic and operational objectives of an E&P company. The ability to estimate pressures in a basin enable more efficient well construction and acreage acquisitions. With the correlation between overpressure and LOM, kerogen maturity maps can be created using the sonic log. With hundreds of sonic logs scattered throughout the basin, the accuracy and veracity of these maps could quickly surpass the USGS study. Knowing the kerogen maturity is required for calculation of kerogen density and kerogen resistivity. With kerogen density, TOC from the ΔLogR can be translated to TOC volume percent. This leads to knowing the organic porosity which can then be used to calculate the matrix porosity from total porosity readings. Given the porosity, pressure, and resistivity data, the petrophysics team can then determine oil saturations using a kerogen resistivity model. Mapping these components onto the basin with overlaying maps of production histories and completions methods allows for the

recognition of the critical contributing factors on a horizon by horizon basin for successful wells. These maps, with the pressure calculations embedded in their foundation, can serve as an important weapon in an E&P's arsenal to execute their strategic mission.

REFERENCES

Barker, C. 2015 Personal Communication via email. 01 December 2015.

Bowers, G. 1995. Pore Pressure Estimation from Velocity Data: Accounting for Overpressure Mechanisms besides Undercompaction. *SPE Drilling & Completions Journal,* Volume 10 (2), 89-95. SPE-27488-PA.

Carpentier, B., Huc, A., and Bessereau, G. 1991. Wireline Logging and Source Rocks—Estimation of Organic Carbon Content by the CARBOLOG ® Method. *The Log Analyst,* May-June 1991, 279-297.

Cox, D. 1995. Distribution and Generation of the Overpressure System, Eastern Delaware Basin, Western Texas and Southern New Mexico: Discussion. *AAPG Bulletin,* Volume 79 (12), 1822.

Eaton, B. 1969. Fracture Gradient Prediction and Its Application in Oilfield Operations. *SPE Journal of Petroleum Technology,* Volume 21 (10), 1353-1360. SPE-2163-PA.

Eaton, B. 1972. The Effect of Overburden Stress on Geopressure Prediction from Well Logs. *SPE Journal of Petroleum Technology,* Volume 24 (08), 929-934. SPE-3719-PA.

Eaton, B. 1975. The Equation for Geopressure Prediction from Well Logs. Presented at the Fall Meeting of the Society of Petroleum Engineers of AIME, Dallas, Texas, 28 September-1 October. SPE-5544-MS.

Eslinger, E. and Pevear, D. 1988. Clay Minerals for Petroleum Geologists and Engineers Short Course no. 22. Society for Sedimentary Geology.

Hood, A., Gutjahr, C., and Heacock, R. 1975. Organic Metamorphism and the Generation of Petroleum. AAPG Bulletin, Volume 59 (6), 986-996.

Hottmann, C. and Johnson, R. 1965. Estimation of Formation Pressures from Log-Derived Shale Properties. *Journal of Petroleum Technology,* Volume 17 (06), 717-722. SPE-1110-PA.

Hubbert, M. and Rubey, W. 1959. Role of Fluid Pressure in Mechanics of Overthrust Faulting. Bulletin of the Geologic Society of America, Volume 70, 115-166.

Issler, D., Bloch, J., and Katsube, T. 2002. Organic Carbon Content Determined from Well Logs: Examples from Cretaceous Sediments of Western Canada. Geological Survey of Canada, Open File 4362.

Jones, R.S. Jr., Pownall, B., and Franke, J. 2014. Estimating Reservoir Pressure from Early Flowback Data. Presented at Unconventional Resources Technology Conference, Denver, Colorado 25-27 August 2014. URTeC: 1934785

Juhasz, I. 1986. Assessment of the distribution of shale, porosity and hydrocarbon saturation in shaly sands. SPWLA 10th European Formation Evaluation Symposium, Aberdeen, 22 April 1986, Pages AA1-15.

Lane, R. and Macpherson, L. 1976. A Review of Geopressure Evaluation from Well Logs-Louisiana Gulf Coast. *Journal of Petroleum Technology*, Volume 28 (09), 963-971. SPE-5033-PA.

Lee, M. and Williams, D. 2000. Paleohydrology of the Delaware Basin, Western Texas: Overpressure Development, Hydrocarbon Migration, and Ore Genesis. *AAPG Bulletin,* Volume 84 (7), 961-974.

Luo, M. and Baker, M. 1995. Distribution and Generation of Overpressure System, Eastern Delaware Basin, Western Texas, and Southern New Mexico: Reply. *AAPG Bulletin*, Volume 79 (12), 1823-1824.

Luo, M., Baker, M., and LeMone, D. 1994. Distribution and Generation of Overpressure System, Eastern Delaware Basin, Western Texas, and Southern New Mexico. *AAPG Bulletin*, Volume 78 (9), 1386-1405.

Lou, X. and Vasseur, G. 1992. Contributions of Compaction and Aquathermal Pressuring to Geopressure and the Influence of Environmental Conditions. *AAPG Bulletin*, Volume 76 (10), 1550-1559.

Osborne, M., and Swarbrick, R. Mechanisms for Generating Overpressure in Sedimentary Basins: A Reevaluation. *AAPG Bulletin,* Volume 81 (6), 1023-1041.

Passey, Q., Creaney, S., and Kulla, J. 1990. A Practical Model for Organic Richness from Porosity and Resistivity Logs. *AAPG Bulletin*, Volume 74 (12), 1777-1794.

Passey, Q., Bohacs, K., Esch W. et al. 2012. My Source Rock is Now My Reservoir-Geologic and Petrophysical Characterization of Shale-Gas Reservoirs. AAPG Search and Discovery Article #80231.

Pawlewicz, M., Barker, C., and McDonald, S. 2005. Vitrinite reflectance data for the Permian Basin, West Texas and Southeast New Mexico. 2005-1171, USGS, (June 2005).

Schlumberger. 2013. Log Interpretation Charts, 2013 Edition. 2013. Schlumberger, Houston.

Schlumberger. 1989. Log Interpretation Principles/Applications, 3rd Printing. Schlumberger Educational Services, Houston.

Schmoker, J. 1979. Determination of Organic Content of Appalachian Devonian Shales from Formation-Density Logs. *AAPG Bulletin*, Volume 63 (9), 1504-1537.

Swarbrick, R. 1995. Distribution and Generation of the Overpressure System, Eastern Delaware Basin, Western Texas and Southern New Mexico: Discussion. *AAPG Bulletin*, Volume 79 (12), 1817-1821.

Terzaghi, K., Peck, B., and Mesri, G. 1996. Soil Mechanics in Engineering Practice, 3rd Edition. John Wiley and Sons Inc., New York.

Timur, A. 1987. Acoustic Logging. In *Petroleum Engineering Handbook*, 3rd ed. H. Bradley, Chap. 51, 51-1 - 51-52. Richardson: Society of Petroleum Engineers.

Van Krevelen. 1950. Graphical-Statistical Method for the Study of Structure and Reaction Processes of Coal. *Fuel*, Volume 29 (12), 269-284.

Vassoyevich, N., Korchagino, Y., Lopatin, N., and Chernyshev, V. 1970. Principal Phase of Oil Formation. International Geology Review Volume 12 (11), 1276-1296.

Ward, J. 2010. Kerogen Density in the Marcellus Shale. Presented at SPE Unconventional Gas Conference, Pittsburg, Pennsylvania. 23-25February. SPE-131767-MS.